Earth-Science Reviews 136 (2014) 96–120

Contents lists available at ScienceDirect

Earth-Science Reviews

journal homepage: www.elsevier.com/locate/earscirev

Petrogenesis of Kerguelen mantle plume-linked Early Cretaceous ultrapotassic intrusive rocks from the Gondwana sedimentary basins, Damodar Valley, Eastern India

N.V. Chalapathi Rao [a,*], Rajesh K. Srivastava [a], Anup K. Sinha [b], V. Ravikant [c]

[a] Department of Geology, Centre of Advanced Study, Banaras Hindu University, Varanasi 221005, India
[b] Dr. K.S. Krishnan Geomagnetic Research Laboratory, Indian Institute of Geomagnetism, Jhunshi, Allahabad 221505, India
[c] Indian Institute of Science Education and Research Kolkata, Mohanpur 741252, India

ARTICLE INFO

Article history:
Received 20 June 2013
Accepted 9 May 2014
Available online 29 May 2014

Keywords:
Lamproites
Lamprophyres
Rajmahal Traps
Kerguelen plume
Damodar Valley
India

ABSTRACT

Mineral chemistry, bulk-rock geochemistry and radiogenic isotope (Sr and Nd) data of surface and sub-surface samples of early-Cretaceous Kerguelen mantle plume linked ultrapotassic intrusive rocks from previously unstudied localities of Raniganj and Jharia Gondwana sedimentary basins, Damodar Valley, eastern India, are presented. Despite considerable textural diversity and variable mineralogy these rocks display broadly similar geochemistry highlighting their co-genetic nature. Their bulk-geochemical and petrographic characteristics are similar to those of ultramafic lamprophyres and liquidus mineral composition are closer to that of lamproites and are strikingly comparable to ultrapotassic rocks reported from the Denizli region (Western Anatolia, Turkey), Karinya Syncline and Mt. Bundey (Australia) and the Polayapalle, eastern Dharwar craton (southern India). Incompatible trace element concentrations (e.g., Sr, Zr, Nb, Ta etc.) and their ratios (Ce/Pb, Nb/U, Nb/Yb, Th/Yb) reveal limited influence of crustal contamination and involvement of a predominantly within-plate (plume) and minor subduction-derived components in their magmas. Initial Sr–Nd isotopic ratios of the Damodar Valley ultrapotassic intrusives suggest their derivation from source regions with long term incompatible element enrichment relative to that of Bulk Earth which are very different from those of (i) kimberlites and orangeites from India and southern Africa and (ii) primitive Kerguelen plume component but indistinguishable from those of the pristine Kerguelen mantle plume derived basalts. The depleted mantle (T_{DM}) model ages (0.95–1.4 Ga) of the Damodar Valley ultrapotassic rocks are strikingly similar to (i) those of the Deccan-age orangeites from the Bastar craton, central India, and (ii) the emplacement ages (1.1–1.4 Ga) of kimberlites and lamproites from the eastern Dharwar craton, southern India. The Gondwana ultrapotassic rocks represent small degree-partial melts derived from a depleted harzburgitic source subsequently metasomatised by carbonate- and rutile-rich fluids/melts, presumably derived from Kerguelen plume, within the garnet stability field at lithospheric depths. A temporal difference of ~500 Ma in the source enrichment of Jharia and Raniganj ultrapotassic intrusives, coupled with their distinct incompatible element signatures, bring out involvement of a heterogeneous mantle in their genesis.

Contents

* Corresponding author. Tel.: +91 9935647365.
E-mail address: nvcr100@gmail.com (N.V. Chalapathi Rao).

http://dx.doi.org/10.1016/j.earscirev.2014.05.012
0012-8252/

1. Introduction

There is a growing evidence for a strong link, vis-à-vis mantle plumes, between small-volume, volatile-rich and potassic magmas (such as kimberlites, orangeites, lamproites, and lamprophyres), which are considered as Small Igneous Provinces (SIPs; Schissel and Ernst, 2013) and large-volume, continental flood basalt dominated Large Igneous Provinces (LIPs) in many continents throughout the geological time scale (e.g., Kent et al., 1998; Luttinen et al., 2002; Griffin et al., 2005; Gibson et al., 2006; Ernst and Srivastava, 2008; Chalapathi Rao and Lehmann, 2011). However, their exact temporal (cause vs consequence) and petrogenetic relationships as well as links to associated mantle plumes (contributors of heat or melt or both) remain unclear and are hotly debated (see Kent et al., 1997; Griffin et al., 2005; Guarino et al., 2013).

The early-Cretaceous (~117–118 Ma) Rajmahal–Sylhet basalts in eastern India, and Bunbary basalts in SW Australia and Antarctica, all

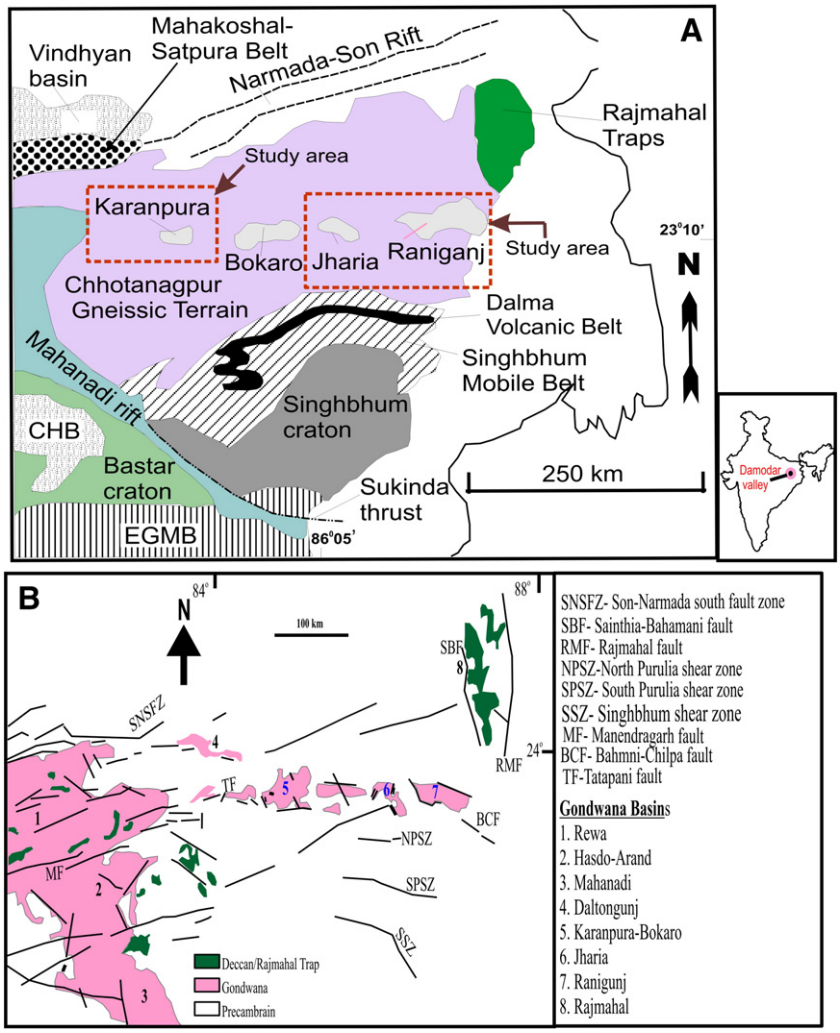

Fig. 1. (A) A generalised geological map of the Chhotanagpur Gneissic Complex showing the disposition of Gondwana coal fields of Ranigunj, Jharia, Bokaro and Karanpura in the Damodar valley (modified from Acharyya, 2003). CHB = Chhattisgarh basin and EGMB = Eastern Ghats Mobile belt. (B) Geological sketch map depicting various tectonic elements in the Chhotanagpur Gneissic Complex and its environs (modified after Kent et al., 1997).

of which collectively constitute a LIP, are widely related to the opening up of the Indian ocean caused by a large mantle plume sourced from the hotspot presently beneath the Kerguelen Plateau in the southern Indian ocean (e.g., Mahoney et al., 1983; Baksi et al., 1987; Storey et al., 1989; Kent et al., 1997; Frey et al., 2002; Srivastava et al., 2005; Srivastava and Sinha, 2007; Ghatak and Basu, 2011). In the eastern and NE India, a variety of alkaline rock-carbonatitic complexes (Sung Valley, Samchampi, Jasra etc.) located in the Shillong Plateau and Mikir Hills (towards the eastern side of the presently exposed Rajmahal basalts) as well as several ultrapotassic dykes and sills (towards the western side of the presently exposed Rajmahal basalts) within the Gondwana coal fields of the Damodar Valley in the Chhotanagpur Gneissic Terrane are widely considered to be an integral component of the early Cretaceous Rajmahal–Bunbary LIP and have been linked to the Kerguelen mantle plume activity (e.g., Veena et al., 1998; Srivastava et al., 2005; Srivastava and Sinha, 2007; Melluso et al., 2010, 2012; Ghatak and Basu, 2013).

The Cretaceous ultrapotassic intrusives emplaced in the Gondwana sedimentary basins and rarely at their adjacent Precambrian basement rocks are well-known for their petrological complexity since more than a century and are widely regarded as "difficult to classify" rocks. Their nomenclature is not straight-forward and over the years have been variously referred to as mica-traps, mica-peridotites, lamprophyres, glimmerites, orangeites and lamproites in the literature (e.g., Blandford, 1861; Bose, 1888; Mukherjee, 1961; Sarkar et al., 1980; Gupta et al., 1983; Middlemost et al., 1988; Rock and Paul, 1989; Rock et al., 1992; Basu et al., 1997; Kent et al., 1998; Jia et al., 2003; Mitchell, 2006, 2007; Mitchell and Fareeduddin, 2009; Srivastava et al., 2009). Apart from these classification-related issues, there is also a marked divergence in the petrological models proposed for the genesis of these

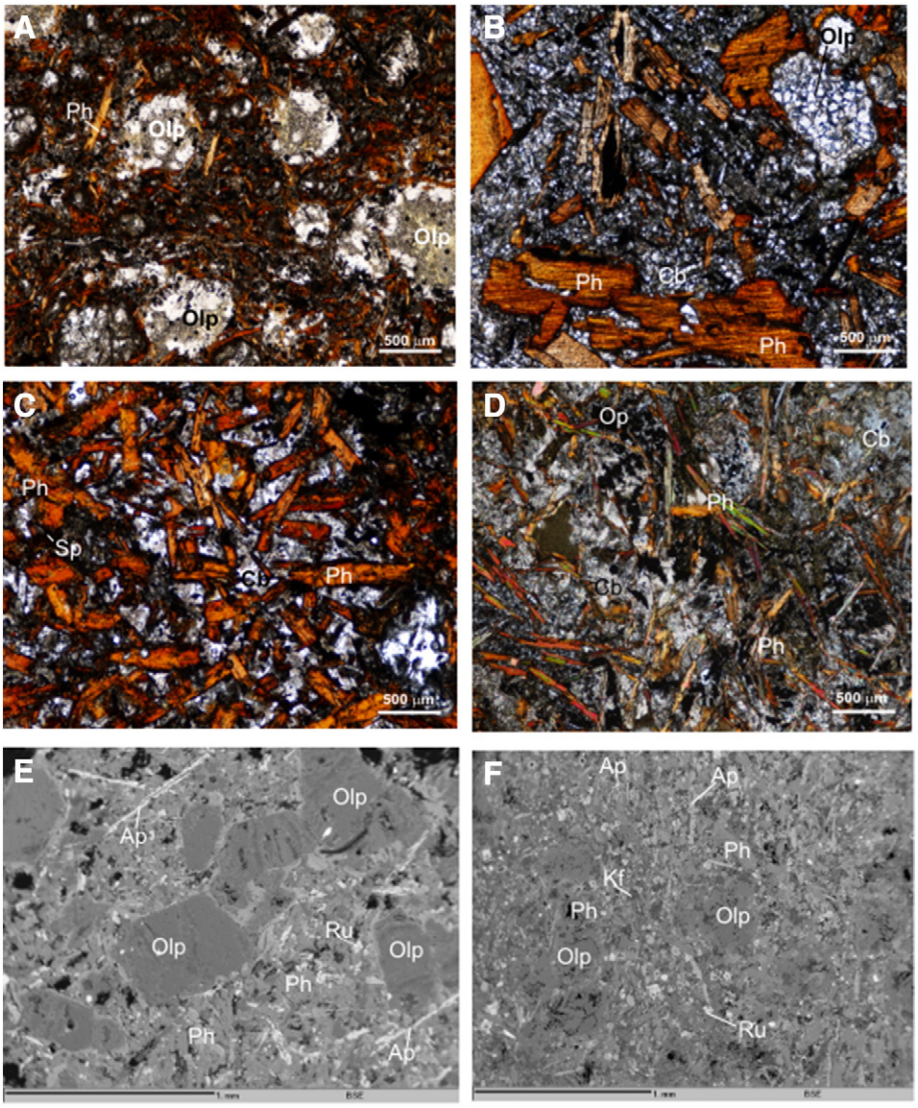

Fig. 2. (A) Pseudomorphosed rounded to sub-rounded olivine macrocrysts displaying a glomeroporphyritic texture (Plane polarised light; JH8/BH1); (B) Unaltered phenocrystal mica phlogopite is the predominant phase in all of the studied thin sections (Plane polarised light; JH8/7B); (C) Microphenocrysts of phlogopite exhibiting an interstitial texture (Plane polarised light; RGM09/13);(D) Carbonate is an abundant accessory in the Jharia as well as Raniganj samples (Plane polarised light; RGM09/13);(E) Back-scattered electron image (BSE) showing subhedral to euhedral pseudomorphosed olivine macrocrysts embedded in a matrix dominated by phlogopite. Acicular laths of apatite and rutile constitute important accessories (Plane polarised light; RGM09/12); (F) Modal apatite is relatively more in abundance in the Raniganj samples (BSE; RGM09/10); (G) >1 mm long phlogopite laths showing preferential alignment in a groundmass consisting of K-feldspar, quartz and rutile (BSE; RGM09/16); (H) Perfectly euhedral groundmass spinels and corroded microphenocrystal phlogopite laths in RGM09/1 (BSE); (I) Groundmass anhedral to subhedral rutile aggregates and prismatic as well as acicular apatite are a conspicuous feature in some samples (BSE; RGM09/1); (J) A higher magnification image showing K-rich titanate, having a composition close to that of potassium triskaidecatitanate ($K_2Ti_{13}O_{27}$), (BSE; JH8/BH2); (K) Prismatic aggregates of amphibole and acicular laths of pyroxene are prominently found in JH8/BH2 sample (BSE); and (L) Apatite occurring as irregular inclusions within a zoned phlogopite microphenocryst (BSE; JH8/BH2). [Abbreviations: Olp = olivine pseudomorph; Ph = phlogopite; Cb = carbonate; Sp = spinel; Ru = rutile; Ap = apatite; Kf = K-feldspar; Srp = serpentine; Am = amphibole; Py = pyroxene].

rocks. For example, Middlemost et al. (1988) identified a minette–lamproite association from the Damodar Valley and recognised their evolution from a common primary magma generated from depths of ~100 km from the upper mantle. Rock et al. (1992) proposed a bulk-compositional similarity of the Jharia ultrapotassic rocks with that of diamondiferous lamproites from the Argyle, Western Australia. Kent et al. (1998) highlighted that Jharia ultrapotassic rocks have more mineralogical similarities to archetypal orangeites from Kapvaal craton, southern Africa, than lamproites. Kumar et al. (2003) show that Sr, Nd and Pb isotopic composition of an early Cretaceous "Group II kimberlite" from the Jharia area to be similar to those of the Cretaceous Broken Ridge, Kerguelen Plateau and Cenozoic pristine Kerguelen plume derived basalts and deduce that Kerguelen hot spot to be directly responsible for mafic and ultrapotassic magmatism in eastern India. Srivastava et al. (2009) invoked a unique geodynamic setting involving (i) metasomatically veined and thinned lithosphere and (ii) the inheritance of ancient (Archaean) subducted component in deciding the diverging petrological and geochemical characters (those of aillikites and cratonic magmas such as lamproites and orangeites) for some ultrapotassic rocks from the Jharia area. Mitchell and Fareeduddin (2009) inferred two of the ultrapotassic rocks from the Raniganj coal field (from Gourangdih and Begonia areas) to be peralkaline lamproites and envisaged their generation from partial melting of ancient, mineralogically complex veins in the lithospheric mantle. Mitchell and Fareeduddin (op.cit) further concluded that none of the ultrapotassic rocks from the Damodar Valley can be regarded as minettes or orangeites or aillikites.

In the present study, we report and discuss mineral chemical, bulk-rock geochemical and limited radiogenic isotopic (Sr and Nd) data for surface, underground mine and borehole samples of twenty one ultrapotassic intrusive rocks collected from ten wide-spread and previously unstudied localities of Raniganj and Jharia sedimentary basins, Damodar Valley, eastern India. These samples (i) enlarge the existing petrological and geochemical data-sets on these rocks, (ii) permit to constrain tectonic setting of emplacement, (iii) evaluate the relative contributions of sub-continental lithsopheric mantle and sub-lithosphere (Kerguelen plume derived) mantle in the petrogenesis of their magmas, and (iv) provide a rare opportunity to investigate the composition of the continental mantle in newer domains from the Damodar Valley and thereby contribute to the existing geodynamic models, involving mantle plume–lithosphere interactions, for the genesis of such exotic rocks.

2. Background geological information

The eastern Indian shield comprises Singhbhum craton, Singhbhum mobile belt, Chhotanagpur Gneissic Terrain (CGT) (Fig. 1A) and the

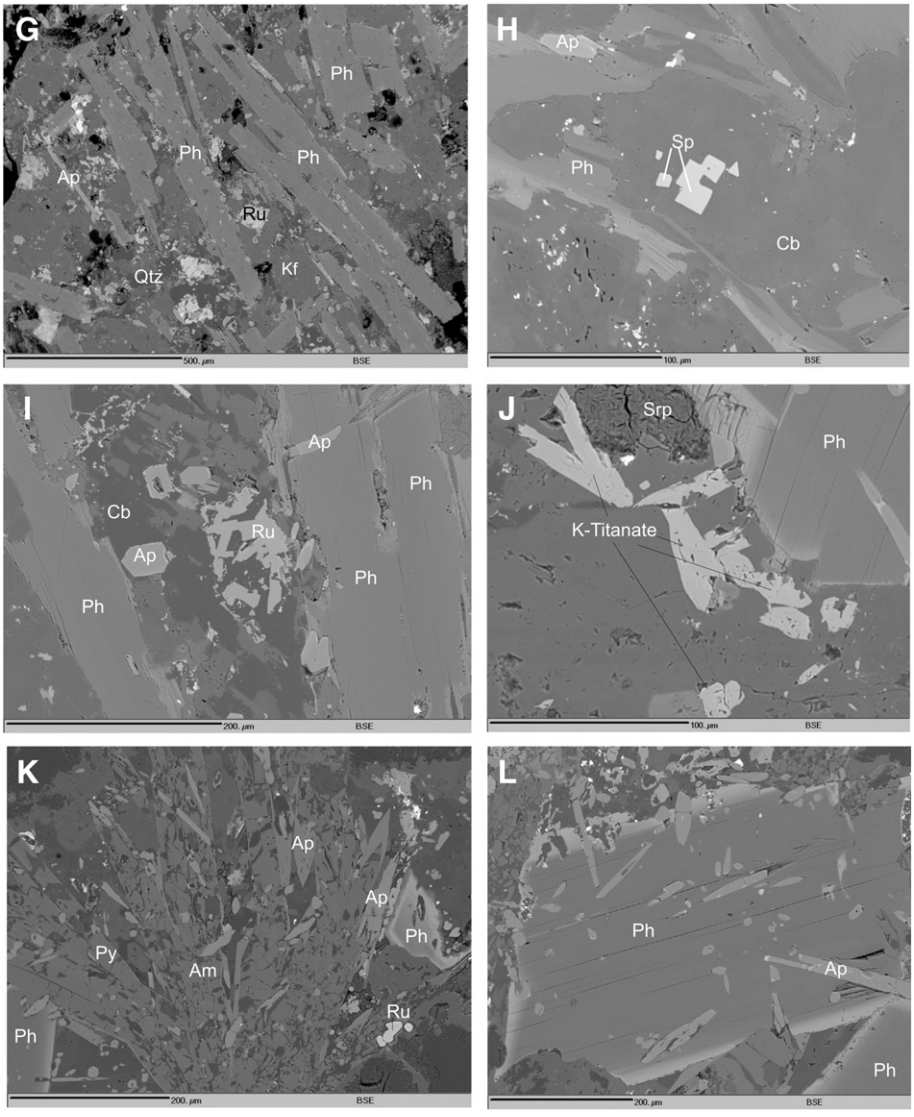

Fig. 2 (*continued*).

Table 1
Mineral chemistry (oxide wt.%) of phlogopite from the samples under study. FeO = total iron.

Oxide wt.%	RGM09/12 core	RGM09/12 rim	RGM09/12 core	RGM09/12 rim	RGM09/16 core	RGM09/16 rim	RGM09/16 core	RGM09/16 rim	RGM09/1 core	RGM09/1 rim	RGM 09/1 core	RGM 09/1 rim
SiO_2	38.57	37.72	35.67	35.89	37.17	36.60	37.70	37.06	37.33	37.13	35.69	37.24
TiO_2	6.94	7.77	7.89	9.58	9.44	9.05	9.57	8.93	8.72	10.09	9.06	9.13
Al_2O_3	10.88	11.41	11.09	11.85	10.76	9.76	9.45	10.46	12.78	11.65	12.23	12.77
FeO	7.78	7.83	14.80	10.68	10.00	12.05	12.02	10.47	6.67	9.90	8.55	6.72
MnO	0.06	0.04	0.12	0.10	0.05	0.07	0.06	0.05	0.03	0.05	0.06	0.03
MgO	18.68	18.14	13.47	14.81	16.95	16.18	15.69	16.82	18.26	16.36	17.46	17.89
CaO	0.00	0.00	0.46	0.01	0.02	0.08	0.05	0.02	0.03	0.15	0.05	0.06
Na_2O	0.32	0.31	0.49	0.32	0.13	0.18	0.27	0.20	0.18	0.22	0.17	0.15
K_2O	9.59	9.59	8.68	9.03	10.15	9.66	10.20	10.03	10.22	10.25	9.97	10.05
Total	92.81	92.80	92.66	92.29	94.66	93.63	95.00	94.03	94.22	95.79	93.24	94.05
Cations for 22 oxygen atoms												
Si	5.747	5.632	5.532	5.471	5.531	5.563	5.650	5.564	5.478	5.459	5.362	5.472
Ti	0.778	0.873	0.920	1.099	1.057	1.035	1.079	1.008	0.963	1.115	1.023	1.009
Al	1.910	2.007	2.026	2.129	1.886	1.748	1.669	1.851	2.211	2.019	2.166	2.210
Fe	0.969	0.978	1.919	1.361	1.244	1.532	1.506	1.315	0.818	1.216	1.074	0.825
Mn	0.008	0.005	0.016	0.013	0.006	0.009	0.008	0.007	0.003	0.006	0.008	0.004
Mg	4.150	4.039	3.114	3.365	3.760	3.667	3.505	3.765	3.994	3.586	3.910	3.919
Ca	0.000	0.000	0.077	0.002	0.004	0.013	0.008	0.003	0.005	0.023	0.008	0.010
Na	0.093	0.089	0.148	0.095	0.039	0.054	0.078	0.057	0.050	0.064	0.050	0.043
K	1.822	1.826	1.716	1.756	1.926	1.872	1.950	1.922	1.912	1.922	1.910	1.884
Total	15.477	15.449	15.468	15.292	15.452	15.492	15.451	15.491	15.435	15.409	15.511	15.377
Mg/(Mg + Fe)	0.81	0.81	0.62	0.71	0.75	0.71	0.70	0.74	0.83	0.75	0.78	0.83

Shillong plateau. Polyphase deformation, metamorphism and magmatism are conspicuous features of the CGT (Mahadevan, 2002; Ghose and Chatterjee, 2008). The exact relationship between Singhbhum craton and Chhotanagpur Gneissic Terrain (CGT) is disputed; whilst some regard CGT as a mobile belt and constitutes a distinct terrane (Ghose, 1983; Mukhopadhyay, 1988; Mahadevan, 2002; Ghose and Chatterjee, 2008 and references therein), many others consider it to be a cratonised mobile belt (Naqvi and Rogers, 1987; Kumar and Ahmad, 2007; Sharma, 2009; Srivastava et al., 2012, 2013). In this study we favour the latter view since i) CGT has an Archaean antiquity whose convergence with the Singhbhum craton in the south gave rise to the Singhbhum mobile belt and medium-grade enclaves of metasediments and basic rocks exclude its mobile belt nature (Sharma, 2009); (ii) occurrences of spinifex textured komatiite, which is characteristic of Archaean terranes, near Daltonganj (Bhattacharya et al., 2010); (iii) presence of potassic intrusives with petrological and geochemical affinities to predominantly cratonic magmas such as orangeites, lamproites and aillikites- (Srivastava et al., 2009) and (iv) Mesoproterozoic metabasite rocks and amphibolites dykes respectively exposed south and north of the Damodar valley show their emplacement in an extensional tectonic regime of intracratonic setting (Ghose et al., 2005; Kumar and Ahmad, 2007). A number of intra-continental faults/shear zones, mostly trend in ENE–WSW to E–W and which controlled the magmatism in the CGT, are conspicuous in the CGT (Fig. 1B). Magnetotelluric investigations show that the present day lithosphere–asthenosphere (LAB) boundary in the Singhbhum craton is thin and at a depth of only 95 km (Shalivahan et al., 2014).

The E–W trending Damodar Valley in the CGT hosts a number of major Gondwana (Permo-Carboniferous) coaliferous sedimentary basins such as Raniganj, Jharia, Karanpura Bokaro, Daltonganj etc. and both extensional and strike-slip regimes have been proposed for their origin (Chakraborty et al., 2003; Ghosh, 2006). Hundreds of mafic (diabase) and ultramafic intrusions (dykes, sills as well as cylindrical bodies) cross-cut the Damodar Valley basins and their basement (Kent et al., 1992; Mukherjee and Ghose, 1999; Mahadevan, 2002). Whereas the earlier dates based on K–Ar technique on mafic as well as ultrapotassic intrusions gave a wide spread range (105–121 Ma; Agarwal and Rama, 1976; Sarkar et al., 1980), Ar–Ar dating gave a much restricted age range of 110–115 Ma for the mafic dykes (Kent et al., 1997, 2002) and 114–116 Ma for the ultrapotassic dykes (Kent et al., 1998; P.R. Renne in Ghatak and Basu, 2013) close to the 117–118 Ma age of the Rajmahal–Sylhet Traps (Baksi, 1995; Ray et al., 2005). However, one of the mafic dykes from the domain viz., Salma dyke has been dated to be of 65 Ma and has been linked to the Deccan event (Kent et al., 2002; Paul, 2005). The Damodar Valley, thus, is the only yet known geological domain in the entire Indian shield which hosts the early Cretaceous Rajmahal- as well as the Late-Cretaceous Deccan-igneous activities.

3. Sampling and analytical techniques

A number of freshest looking surface, underground mine as well as borehole samples (where available) of ultramafic rocks were collected from the J.K. Nagar, Nigah, Kalidaspur, Bhanra West, Lakimata, Shyampur, Jogidih, Sayal and Parbatpura areas of the Jharia and Raniganj coal fields. The GPS co-ordinates and geochemical nature of each sample of this study (as per TAS plot) are provided in Table 9. Chemical composition of the minerals was determined by CAMECA-SX100 CAMECA-SX 100 electron microprobe at the Mineral Resources, Technical University of Clausthal, Clausthal-Zellerfeld, Germany. The analyses were carried out using wavelength dispersive spectrometry. An accelerating voltage of 15 kV (for major elements) 20 kV (for trace elements), a beam current of 50 nA and a beam diameter of 1 μm was used employing TAP, PET and LLIF crystals and a PAP online correction program. Several in-house natural and synthetic standards and were used for calibration. After repeated analyses it was found that the error on major element concentrations is <1% whereas the error on trace elements varied between 5 and 10%.

Whole-rock geochemistry was carried out at the Activation Laboratories, Ancaster, Canada. ICP-OES (Model: Thermo-JarretAsh ENVIRO II) was used to analyse major elements and few trace elements (Sc, V, Ba, Sr, Zr, and Y), whereas ICP-MS (Model: Perkin Elmer Sciex ELAN 6000) was used to determine trace and rare-earth element concentrations. MRG1, W2, DNC1, STM1 and SY3 were used as internal standards and the precision is approximately 5% and 5–10% for the major oxides and trace elements, respectively, when reported at 100× detection limit. Several standards, such as MRG1, W2, DNC1, STM1 and SY3, were analysed to check accuracy and precision. The analytical procedure is detailed by Gale et al. (1997) and available at the Activation Laboratories Ltd. website (http://www.actlabs.com).

The isotopic analyses were conducted at the National Facility for Geochronology and Isotope Geology at the IIT Roorkee, India. For Rb–

RGM 09/8 core	RGM 09/8 rim	RGM 09/10 core	RGM 09/10 core	RGM 09/10 core	RGM 09/10 core	JH8/BH2 core	JH8/BH2 rim	JH8/BH2 core	JH8/BH2 rim	JH8/7B core	JH8/7B rim	JH8/7B core	JH8/7B rim
37.72	35.37	37.64	37.21	36.37	36.50	34.44	35.75	35.15	33.24	36.31	37.71	39.46	39.55
7.82	8.46	7.25	7.54	7.33	10.48	8.84	8.08	8.62	8.08	5.41	5.48	9.50	9.10
12.02	11.91	7.23	7.62	8.62	12.21	12.52	11.41	12.69	7.80	16.74	16.36	12.02	12.33
6.75	10.74	11.13	11.95	12.37	6.39	7.80	10.14	7.35	29.35	12.89	12.13	5.22	4.99
0.04	0.05	0.04	0.05	0.05	0.02	0.03	0.07	0.02	0.18	0.00	0.02	0.00	0.00
19.02	17.69	19.43	19.21	19.31	17.76	17.96	17.45	18.05	6.78	14.32	14.47	18.37	19.06
0.02	0.19	0.05	0.12	0.05	0.02	0.04	0.02	0.04	0.04	0.07	0.07	0.00	0.08
0.14	0.17	0.17	0.08	0.07	0.12	0.19	0.13	0.12	0.11	0.23	0.16	0.17	0.17
10.54	10.06	10.20	10.13	9.38	10.64	10.23	10.40	10.30	9.71	10.16	10.50	10.71	10.65
94.07	94.64	93.13	93.91	93.54	94.13	92.05	93.45	92.35	95.29	96.13	96.89	95.44	95.93
5.556	5.304	5.750	5.662	5.546	5.386	5.248	5.418	5.314	5.476	5.352	5.486	5.667	5.642
0.867	0.954	0.833	0.863	0.841	1.162	1.013	0.921	0.981	1.001	0.600	0.599	1.026	0.977
2.086	2.105	1.301	1.367	1.549	2.124	2.249	2.039	2.262	1.514	2.908	2.804	2.034	2.073
0.832	1.347	1.422	1.520	1.577	0.788	0.994	1.286	0.929	4.042	1.588	1.475	0.626	0.595
0.005	0.006	0.005	0.007	0.006	0.002	0.003	0.009	0.003	0.025	0.000	0.002	0.000	0.000
4.177	3.955	4.427	4.358	4.389	3.906	4.078	3.942	4.069	1.664	3.146	3.137	3.932	4.054
0.003	0.030	0.009	0.020	0.008	0.004	0.007	0.003	0.006	0.008	0.011	0.011	0.000	0.012
0.039	0.051	0.050	0.023	0.019	0.035	0.057	0.038	0.035	0.034	0.065	0.046	0.048	0.047
1.980	1.924	1.988	1.965	1.824	2.002	1.988	2.011	1.987	2.040	1.911	1.948	1.961	1.937
15.544	15.676	15.785	15.786	15.760	15.409	15.637	15.666	15.586	15.803	15.582	15.509	15.294	15.337
0.83	0.75	0.76	0.74	0.74	0.83	0.80	0.75	0.81	0.29	0.66	0.68	0.86	0.87

Sr and Sm–Nd isotopic analyses, the USGS rock reference samples BCR 2 and W2 were analyzed along with the samples to check the accuracy of the procedure. Isotopic analyses were carried out on a Thermo Finnigan Triton T1 thermal ionisation mass spectrometer, in static multicollector mode as outlined by Ravikant (2010). Mass fractionation corrections in Sr and Nd isotopic analyses were done with $^{86}Sr/^{88}Sr = 0.1194$ and $^{146}Nd/^{144}Nd = 0.7219$, respectively. The precision of $^{87}Sr/^{86}Sr$ (0.03%) and $^{143}Nd/^{144}Nd$ (0.01%) ratios are the external precisions based on replicate determinations of standards; precision on the $^{87}Rb/^{86}Sr$ ratio is 1% and on the $^{147}Sm/^{144}Nd$ ratio is 0.3% by IDTIMS. During the period of this study, the mean $^{87}Sr/^{86}Sr$ ratio was 0.71026 ± 0.00008 (2σ, n = 21) for the NBS 987 Sr standard and $^{143}Nd/^{144}Nd$ ratio for the GSJ JNdi-1 standard (Tanaka et al., 2000) was 0.512108 ± 0.000020 (2σ, n = 23). The total procedural blank was <0.7 ng for Sr, <0.2 ng for Rb and <0.5 ng for Nd. The Rb–Sr and Sm–Nd-isotopic data are given in Table 11; Rb, Sr, Sm and Nd concentrations were calculated offline by a double spike correction program kindly provided by Ernst Hegner, Ludwig-Maximilans University, Munich, Germany.

4. Petrography and mineral chemistry

Both optical microscopic as well as electron micro beam (Back Scattered Electron images) techniques have been deployed to characterise mineralogy of the samples (Fig. 2A–L). Pseudomorphosed olivine, mica (phlogopite–biotite), clinopyroxene (diopside), amphibole (arfvedsonite, eckermanite and richterite), Cr-spinel, potassium-feldspar, carbonates (calcite and ferroan dolomite), Sr-rich apatite, niobian rutile, Mg-ilmenite, chlorite, serpentine, quartz and iron oxides/sulphides in varying proportions constitute the overall mineralogy of the studied samples. Pseudomorphosed olivine, phlogopite and carbonate minerals are particularly abundant as major phases in all the samples whereas rest others occur as minor to accessory phases. It should be mentioned here that K-rich titanate (having a composition close to that of potassium triskaidecatitanate $K_2Ti_{13}O_{27}$) grains have also been recently reported (Chalapathi Rao et al., 2013a) from one of the samples (JH8/BH2) of this study. A textural diversity, ranging from porphyritic through glomeroporphyritic to interstitial and flow textures (Fig. 2), is portrayed by the studied samples. Individual description of each of the minerals is provided below together with a discussion of their respective mineral compositions.

4.1. Olivine

No fresh olivine has been observed and only its pseudomorphs exist and occur up to 700 μm (Fig. 2A, B and E). Their identity has been inferred from their shape (subrounded to subhedral) as well as from the associated alteration products (serpentine, carbonate and chlorite) and finer-grained opaque minerals that are often concentrated along their edges. At places, glomeroporphyritic aggregates of psedomorphosed olivine are also noticed.

4.2. Mica

It is the most pristine major phase in all the studied samples and occurs as plates and tabular laths usually in a size range of 200 μm to 700 μm (Fig. 2A–D). Very coarse-grained (>1 mm) micas are also noticed in a few samples (Fig. 2G) and some them are corroded (Fig. 2H) and a few are strongly zoned (Fig. 2L). A considerable proportion of micas are characterised by a deep reddish-tinge which is considered to be a characteristic feature of titanium-rich phlogopite (Mitchell, 1995) which is further corroborated by their composition (TiO_2 up to 10.88 wt.%; Table 1). Whereas the studied micas are predominantly phlogopite, some of those from the Jharia ultrapotassic rocks, reported earlier by us (Srivastava et al., 2009), are biotites (not shown). The compositions of micas of this study (Fig. 3A) reveal the following aspects: (i) most of their cation sum of Si and Al is typically less than 8 atoms per 23 oxygens showing apparent tetrahedral deficiencies and some Fe^{3+} very likely occurs in IV fold site (tetraferriphlogopites), (ii) a great majority of them display increasing iron (Fig. 3B) and titania (Fig. 3C) with a depletion in alumina typical of those found in lamproites and to some extent in orangeites, (iii) only a very few micas show compositional trends of minette/alnoite (ultramafic lamprophyres) whilst none of them show evolutionary trends of archetypal kimberlite and (iv) micas from Raniganj and Jharia of this study are indistinguishable in their overall composition. The mica compositions reported for Raniganj samples by Mitchell and Fareeduddin (2009) are also plotted along with and some of them show extreme iron enrichment (Fig. 3B) compared to the micas of this study. The micas from the Mesoproterozoic lamproites from the Eastern Dharwar craton, southern India, show an overall compositional similarity to those from the Jharia and Ranigunj samples (Fig. 3A–C).

4.3. Spinel

Near perfect euhedral spinels of 15–20 μm size are found mostly found as discrete grains in the groundmass (Fig. 2H) and are compositionally Mg-chromites (Table 2). Their compositional variation, when projected on to the front face of a reduced Fe spinel prism, follows two distinct trends (Fig. 3D): (i) All the Jharia and a few Raniganj spinels display a magnesian-ulvöspinel-magnetite trend (T1), unique to spinel in archetypal kimberlites and (ii) many of the Raniganj spinels, and none from those of Jharia, show a titanian-magnetite trend (T2) which is similar to trend displayed by spinel from orangeites and lamproites (Mitchell, 1995) and also those from basalts (see Roeder and Schulze, 2008). Interestingly, the spinel from Raniganj samples reported by Mitchell and Fareeduddin (2009) are predominantly confined to the T2 field (see Fig. 3D) demonstrating their overall extensive compositional variation. The spinels from the Eastern Dharwar craton lamproites in comparison, have relatively much higher iron and lower titanium concentrations (see Fig. 3D).

4.4. Clinoyroxene

Clinopyroxene is noticed only in a few Jharia samples and when present it occurs as prismatic or lath shaped crystals of up to 400 μm in the matrix (Fig. 3K). It is compositionally a relatively pure diopside

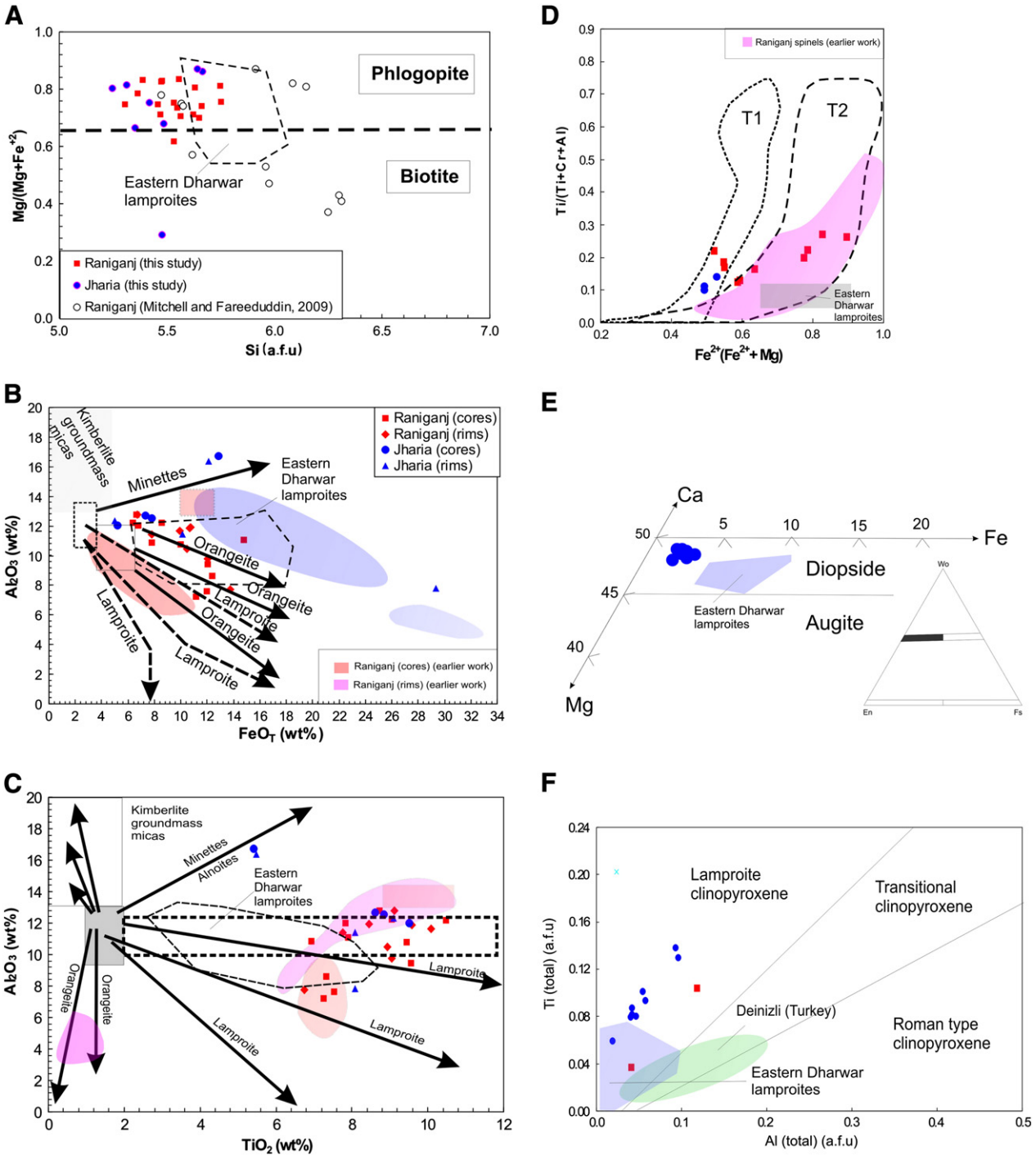

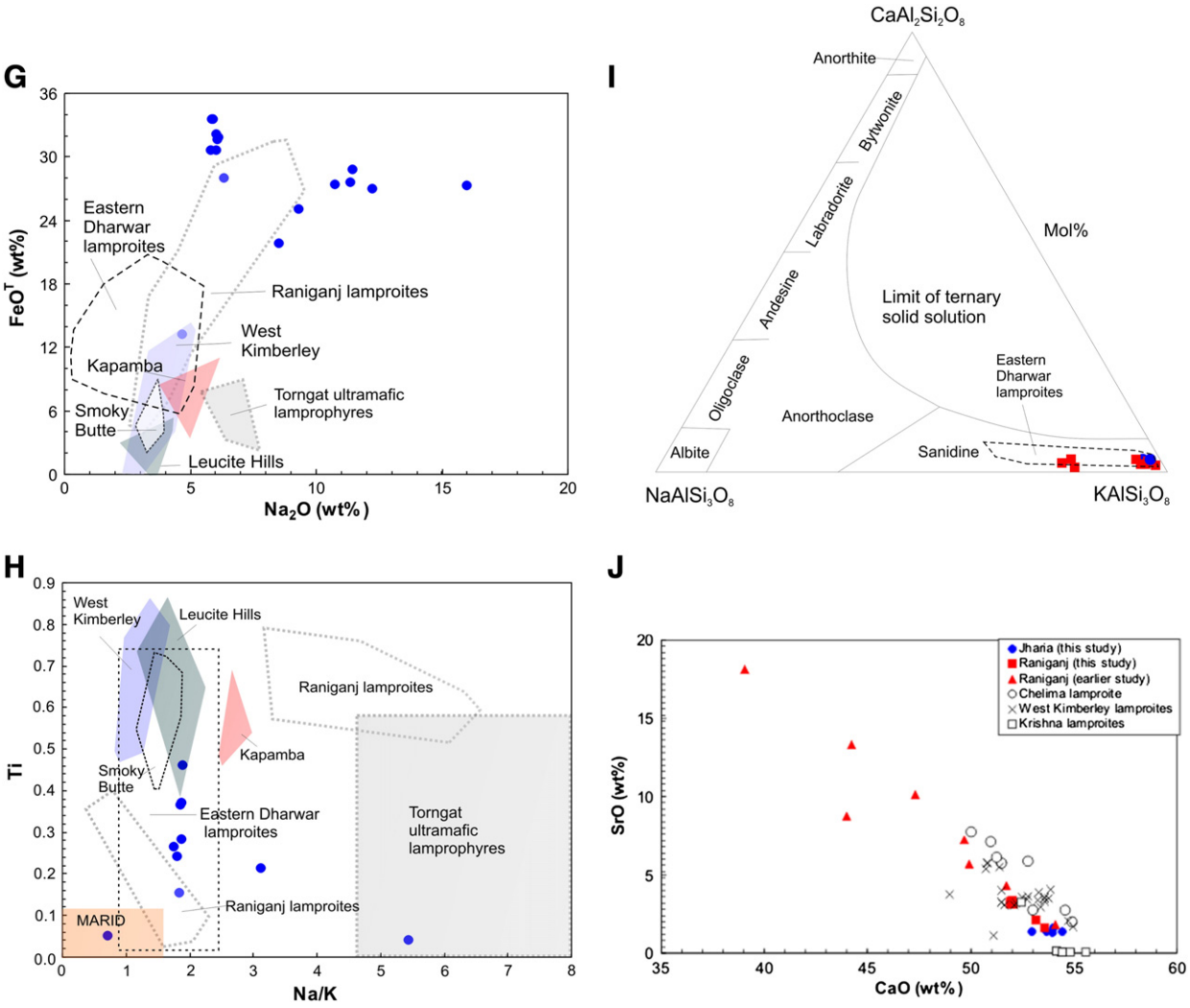

Fig. 3. (A) Si (atoms per formula unit) versus Mg/(Mg + Fe) classification diagram for mica composition (after Reider et al., 1998). Compositional field of micas from Eastern Dharwar lamproites is from Chalapathi Rao et al. (2004, 2010) and Paul et al. (2007). (B) FeO_T (wt.%) versus Al_2O_3 (wt.%) compositional variation of phlogopite in the studied samples. Compositional fields and trends for micas from kimberlite, lamproite, orangeite and minette are taken from Mitchell (1995); compositional field of micas from Raniganj (cores and rims; earlier work) is from Mitchell and Fareeduddin (2009). Compositional field of micas from Eastern Dharwar lamproites is from Chalapathi Rao et al. (2004, 2010) and Paul et al. (2007). Symbols are the same as in Fig. 3A. (C) Al_2O_3 (wt.%) versus TiO_2 compositional variation of phlogopite in studied samples. Compositional fields and trends are from Mitchell (1995) and compositional field of micas from Raniganj (cores and rims; earlier work) is from Mitchell and Fareeduddin (2009). Compositional field of micas from Eastern Dharwar lamproites is from Chalapathi Rao et al. (2004, 2010) and Paul et al. (2007). Symbols are the same as in Fig. 3A. (D) Compositional variation of spinel from the Raniganj and Jharia samples of this study projected onto the front face of a reduced spinel prism. Compositional fields and trends for spinel from kimberlites (T1) and lamproites (T2) are from Mitchell (1995). Compositional field for Raniganj spinels (earlier work) is from Mitchell and Fareeduddin (2009). The field of Eastern Dharwar lamproite spinels is from the authors unpublished data of Ramadugu lamproites. Symbols are the same as in Fig. 3A. (E) Wollastonite (Wo)—Enstatite (En)—Ferrosilite (Fs) classification diagram (after Morimoto et al., 1988) for clinopyroxene in JH8/BH2 sample of this study. The field of Eastern Dharwar lamproites is from Chalapathi Rao et al. (2010); Paul et al. (2007) and unpublished data of the authors. (F) Al (atoms per formula unit) versus Ti (atoms per formula unit) classification plot for clinopyroxene of this study. The field of Eastern Dharwar lamproites is from Chalapathi Rao et al. (2010); Paul et al. (2007) and unpublished data of the authors. Other fields are taken from Mitchell and Bergman (1991), Conticelli (1988) and Semiz et al. (2012). The data for clinopyroxene from Raniganj is taken from Mitchell and Fareeduddin (2009). Symbols remain the same as in Fig. 3A. (G) Na_2O (wt.%) versus FeO_T (wt.%) compositional variation of amphiboles in JH8/BH2 sample of this study. Compositional field of Eastern Dharwar lamproites is from Chalapathi Rao et al. (2004, 2010) and Paul et al. (2007). Compositional fields for various amphiboles from other lamproites are taken from Mitchell and Bergman (1991) and Tappe et al. (2004); the field for Raniganj rocks is from Mitchell and Fareeduddin (2009). (H) Ti versus Na/K (a.p.f.u) compositional variation of amphiboles from JH8/BH2 sample of this study. Compositional field of Eastern Dharwar lamproites is from Chalapathi Rao et al. (2004, 2010) and Paul et al. (2007), field of Raniganj is from Mitchell and Fareeduddin (2009) and rest other fields are from Mitchell and Bergman (1991) and Tappe et al. (2004). (I) Compositions of the feldspar minerals in the Anorthite–Albite–Orthoclase ternary plot. Symbols remain the same as in (A). Field of the Eastern Dharwar craton lamproites is from Chalapathi Rao et al. (2010) and Paul et al. (2007). (J) CaO (wt.%) versus SrO (wt.%) of apatite from the samples under study. Other data sources: Raniganj (earlier study) = Mitchell and Fareeduddin (2009); Chelima lamproites, southern India = Chalapathi Rao (2007, 2011); West Kimberley lamproites = Edgar (1989) and Krishna lamproites, southern India = Chalapathi Rao et al. (2010).

(Fig. 3E) with a tight compositional range ($Wo_{46.92–49.12}$ $En_{39.37–41.55}$ $Fs_{8.35–10.85}$ $Ac_{1.61–2.34}$; Table 3) and distinct in composition from those of the Eastern Dharwar lamproites (Fig. 3E). Their titania content ranges from 2.81 to 4.63 wt.% whereas the Cr_2O_3 content is less than 0.24 wt.%. Al_2O_3 contents range from 0.91 to 2.18 wt.% and CaO has a compositional range of 23.25 to 24.78 wt.%. In the Al–Ti (Fig. 3F) compositional space the diopside from Jharia show distinct lamproitic affinities, broadly similar to the compositions reported for those from Raniganj by Mitchell and Fareeduddin (2009) and is different from the clinopyroxene reported from other paragenesis such as Roman type and transitional type. The diopside of this study is also compositionally dissimilar to the sodium-rich (Na_2O: 3.36–12.44 wt.%) titanian aegerine augites reported in ultrapotassic rocks from Jharia (Rock et al., 1992) and Raniganj (Mitchell and Fareeduddin, 2009) and the clinopyroxene from Eastern Dharwar lamproites (Fig. 3F).

Table 2
Mineral chemistry (oxide wt.%) of spinel (cores) from the samples under study. FeO and Fe_2O_3 recalculated from stoichiometry.

	RGM 09/8	RGM 09/8	RGM 09/8	RGM 09/8	RGM 09/10	RGM 09/10	RGM 09/1	RGM 09/1	RGM 09/1	RGM 09/1	RGM 09/1	JH8/BH2	JH8/BH2	JH8/BH2	RGM 09/1
SiO_2	0.05	0.01	0.05	0.03	0.10	0.07	0.04	0.01	0.05	0.06	0.05	0.04	0.04	0.08	0.05
TiO_2	9.09	9.37	7.72	7.40	9.93	9.85	9.94	9.79	10.92	10.00	8.87	6.02	6.95	5.23	10.92
Al_2O_3	4.09	3.87	5.07	5.23	1.72	1.78	2.13	2.06	1.00	0.88	2.02	7.28	6.98	7.02	1.00
Cr_2O_3	38.02	37.62	41.00	41.62	31.05	36.02	27.72	28.59	26.33	26.44	30.90	43.00	40.01	41.89	26.33
Fe_2O_3	11.66	12.73	10.47	10.25	21.00	16.385	20.88	20.58	20.88	21.954	19.583	10.20	11.32	12.91	20.88
FeO	26.83	23.67	24.71	24.05	21.90	23.205	31.84	31.84	34.02	36.333	32.229	19.87	21.37	19.20	34.02
MnO	0.00	0.00	0.00	0.00	0.00	0.00	0.00	0.00	0.00	0.04	0.000	0.00	0.00	0.00	0.00
MgO	8.66	10.84	9.46	9.46	11.32	10.70	4.97	4.86	4.01	2.39	5.060	11.56	10.94	11.22	4.01
CaO	0.23	0.08	0.06	0.35	1.06	0.14	0.54	0.56	0.89	0.01	0.170	0.39	0.45	0.75	0.89
Total	98.63	98.19	98.54	98.39	98.07	98.15	98.04	98.28	98.09	98.12	98.88	98.35	98.07	98.30	98.09
Cations for 32 oxygen atoms															
Si	0.013	0.001	0.013	0.008	0.028	0.019	0.002	0.002	0.015	0.019	0.013	0.012	0.012	0.022	0.015
Ti	1.905	1.945	1.602	1.536	2.077	1.955	2.089	2.089	2.422	2.277	1.969	1.219	1.423	1.065	2.422
Al	1.342	1.257	1.649	1.701	0.564	0.589	0.712	0.712	0.347	0.313	0.701	2.313	2.205	2.237	0.347
Cr	8.376	8.208	8.948	9.082	6.829	8.000	6.618	6.618	6.142	6.092	7.208	9.158	8.607	8.960	6.142
V	0.000	0.000	0.000	0.000	0.000	0.000	0.000	0.000	0.000	0.000	0.000	0.000	0.000	0.000	0.000
$Fe^{(iii)}$	2.446	2.643	2.174	2.129	4.396	3.463	4.488	4.488	4.636	5.003	4.127	2.067	2.318	2.628	4.636
$Fe^{(ii)}$	6.253	5.462	5.704	5.550	5.095	5.451	7.793	7.793	8.393	9.201	7.703	4.477	4.863	4.344	8.393
Mn	0.000	0.000	0.000	0.000	0.000	0.000	0.000	0.000	0.000	0.011	0.000	0.000	0.000	0.000	0.000
Mg	3.596	4.461	3.892	3.891	4.694	4.481	2.122	2.122	1.763	1.081	2.224	4.641	4.439	4.525	1.763
Ca	0.070	0.023	0.019	0.103	0.317	0.041	0.176	0.176	0.281	0.004	0.054	0.113	0.132	0.218	0.281
Total	24	24	24	24	24	24	24	24	24	24	24	24	24	24	24
$Fe^{2+}/(Fe^{2+}+Mg)$	0.63	0.55	0.59	0.59	0.52	0.55	0.79	0.79	0.83	0.89	0.78	0.49	0.52	0.49	0.83
Ti/(T + Cr + Al)	0.16	0.17	0.13	0.12	0.22	0.19	0.22	0.22	0.27	0.26	0.20	0.10	0.12	0.09	0.27
Cr/(Cr + Al)	0.86	0.87	0.84	0.84	0.92	0.93	0.90	0.90	0.95	0.95	0.91	0.80	0.80	0.80	0.95

4.5. Amphibole

Microphenocrysts of amphibole occurring as slender primatic laths are found in a few samples from the Jharia (Fig. 3E). Compositionally three distinct varieties exist (Table 4) viz., (I) magnesio- to potassic-arfvedsonite (predominant), (ii) ferro-richterite (subordinate) and (iii) ferro-eckermanite (very rare)—all of which are similar in paragenesis to those recorded from the Jharia and Raniganj ultrapotassic rocks by Rock et al. (1992), Kent et al. (1998) and Mitchell and Fareeduddin (2009). However, potassium-titanian ferroan pargasite variety of amphibole reported by Middlemost et al. (1988) from Barakar ultrapotassic rocks is not found. The Jharia amphiboles of this study are extremely

Table 3
Mineral chemistry (oxide wt.%) of pyroxene (core) in the samples under study. Fe_2O_3 is calculated from stoichiometry.

Oxide wt.%	1	2	3	4	5	6	7	8	9
	JH8/BH2	JH8/BH2	JH8/BH2	JH8/BH2	JH8/BH2	JH8/BH2	JH8/BH2	JH8/BH2	JH8/BH2
SiO_2	48.44	48.10	48.25	48.70	48.33	48.55	49.20	49.68	49.05
TiO_2	4.63	4.87	3.78	3.75	2.81	3.54	3.28	2.82	2.95
Al_2O_3	2.18	2.09	0.91	0.89	0.92	1.22	1.29	1.03	0.41
Cr_2O_3	0.24	0.21	0.05	0.14	0.16	0.06	0.16	0.03	0.03
Fe_2O_3	2.61	2.106	5.038	4.973	5.388	4.324	3.96	4.01	5.89
FeO	3.56	4.073	1.737	0.828	0.522	2.286	2.01	3.23	0.64
MnO	0.08	0.05	0.13	0.10	0.09	0.10	0.07	0.11	0.11
MgO	14.24	13.88	14.06	14.90	14.76	14.48	14.50	14.02	14.94
CaO	24.03	24.00	23.78	24.04	24.78	23.88	24.45	23.25	24.17
Na_2O	0.49	0.48	0.64	0.52	0.48	0.51	0.53	0.79	0.45
K_2O	0.01	0.02	0.02	0.00	0.02	0.02	0.02	0.07	0.02
Total	100.49	99.89	98.37	98.84	98.25	98.97	99.48	99.02	98.66
Cations for 6 oxygen atoms									
Si	1.812	1.811	1.867	1.870	1.862	1.849	1.858	1.888	1.891
Ti	0.130	0.138	0.087	0.080	0.082	0.101	0.093	0.081	0.059
Al	0.096	0.093	0.042	0.040	0.042	0.055	0.057	0.046	0.019
Cr	0.007	0.006	0.001	0.004	0.005	0.002	0.005	0.001	0.001
Fe^{3+}	0.073	0.059	0.145	0.142	0.153	0.123	0.111	0.114	0.169
Fe^{2+}	0.111	0.128	0.056	0.026	0.018	0.072	0.063	0.102	0.020
Mn	0.003	0.002	0.004	0.003	0.003	0.003	0.002	0.004	0.004
Mg	0.794	0.779	0.811	0.853	0.848	0.822	0.816	0.794	0.859
Ca	0.963	0.968	0.985	0.989	1.002	0.974	0.989	0.946	0.998
Na	0.035	0.035	0.048	0.039	0.036	0.038	0.039	0.058	0.034
K	0.000	0.001	0.001	0.000	0.000	0.001	0.001	0.003	0.001
Total	4.023	4.019	4.046	4.046	4.049	4.039	4.036	4.036	4.054
Wo	48.68	49.12	48.10	48.19	48.65	47.94	48.95	46.92	47.92
En	40.13	39.54	39.58	41.55	41.16	40.46	40.38	39.37	41.23
Fs	9.40	9.57	9.98	8.35	8.44	9.74	8.74	10.85	9.24
Ac	1.78	1.77	2.34	1.90	1.75	1.86	1.92	2.87	1.61

Table 4
Mineral chemistry (oxide wt.%) of amphiboles (core) of this study. Arfv = arfvedsonite; Fricht = ferrorichterite.

Oxide wt.%	1	2	3	4	5	6	7	8	9	10	11	12	13	14	15	16
	JH8/BH2	JH8/BH2	JH8/BH2	JH8/BH2	JH8/BH2	JH8/BH2	JH8/BH2	JH8/BH2	JH8/BH2	JH8/BH2	JH8/BH2	JH8/BH2	JH8/BH2	JH8/BH2	JH8/BH2	JH8/BH2
SiO_2	45.56	45.85	49.41	50.26	50.20	54.87	46.02	47.22	47.25	47.66	47.20	47.31	50.27	50.44	50.51	50.36
TiO_2	1.94	1.23	2.33	1.81	2.14	0.49	3.02	3.80	2.98	3.01	2.16	2.32	0.34	0.50	2.99	2.96
Al_2O_3	0.12	0.25	0.18	4.63	0.85	10.23	0.40	0.36	0.17	0.17	0.29	0.14	2.23	0.22	0.09	0.08
Cr_2O_3	0.07	0.04	0.04	0.02	0.00	0.01	0.54	1.96	0.20	0.18	0.26	0.40	0.00	0.01	0.25	0.24
Fe_2O_3	10.195	10.272	11.48	2.97	9.557	0.00	7.78	4.16	5.745	4.330	7.04	7.47	6.70	13.07	11.22	12.091
FeO	24.446	24.377	17.27	19.12	18.818	14.23	23.62	24.27	26.961	27.027	24.29	25.18	19.09	17.05	16.91	16.418
MnO	0.96	0.93	0.37	0.27	0.25	0.09	1.08	0.59	0.84	0.87	0.84	0.83	0.34	0.39	0.12	0.13
MgO	0.70	0.76	0.69	0.72	0.34	0.79	1.60	2.03	0.82	0.97	2.11	1.24	0.64	0.71	0.76	0.75
CaO	1.23	1.62	3.56	3.96	4.43	1.97	1.57	1.05	1.13	1.20	1.41	1.29	2.85	3.24	2.74	2.68
Na_2O	5.87	5.91	11.34	8.53	10.75	4.67	6.02	6.33	6.05	6.06	5.80	6.12	9.32	11.45	12.21	12.30
K_2O	4.97	4.89	0.13	4.15	0.71	8.69	4.87	5.08	4.94	4.93	5.06	4.95	4.60	0.04	0.01	0.01
Total	96.05	96.12	96.78	96.43	98.05	96.03	96.51	96.85	97.08	96.41	96.46	97.23	96.37	97.12	97.82	98.02
Cations for 23 oxygens																
Si	7.577	7.650	7.768	7.895	7.802	8.297	7.540	7.641	7.724	7.811	7.702	7.700	8.058	7.891	7.807	7.773
Ti	0.243	0.154	0.275	0.214	0.251	0.052	0.372	0.462	0.366	0.371	0.265	0.283	0.041	0.059	0.347	0.343
Al	0.023	0.049	0.033	0.857	0.155	1.824	0.077	0.069	0.033	0.033	0.057	0.027	0.420	0.040	0.017	0.015
Cr	0.009	0.005	0.005	0.002	0.000	0.001	0.070	0.251	0.026	0.023	0.034	0.051	0.000	0.002	0.031	0.029
$Fe^{(iii)}$	1.276	1.290	1.358	0.351	1.118	0.000	0.959	0.507	0.707	0.534	0.864	0.914	0.808	1.539	1.305	1.404
$Fe^{(ii)}$	3.399	3.401	2.270	2.512	2.446	1.673	3.236	3.285	3.685	3.704	3.314	3.427	2.558	2.230	2.185	2.119
Mn	0.135	0.131	0.049	0.036	0.032	0.012	0.150	0.080	0.116	0.121	0.116	0.114	0.046	0.051	0.016	0.017
Mg	0.175	0.189	0.161	0.168	0.079	0.128	0.391	0.489	0.199	0.237	0.514	0.300	0.152	0.167	0.176	0.173
Ca	0.219	0.179	0.599	0.536	0.738	0.318	0.276	0.182	0.197	0.210	0.246	0.225	0.489	0.542	0.454	0.444
Na	1.893	1.913	3.457	2.597	3.238	1.192	1.911	1.985	1.917	1.925	1.836	1.931	2.895	3.472	3.660	3.681
K	1.053	1.040	0.025	0.831	0.141	1.675	1.018	1.048	1.030	1.030	1.052	1.028	0.532	0.008	0.002	0.001
Total	16.000	16.000	16.000	16.000	16.000	15.172	16.000	16.000	16.000	16.000	16.000	16.000	16.000	16.000	16.000	16.000
	Arfv	Arfv	Fricht	Fricht	Fricht	Ferro-eckermanite	Arfv	Arfv	Arfv	Arfv	Arfv	Arfv	Arfv	Mg-Arfved	Arfv	Arfv

Table 5
Mineral chemistry (oxide wt.%) of feldspars (cores) from the samples under study. FeO is total iron.

	1	2	3	4	5	6	7	8	9	10	11	12	13	14	15
Oxide wt.%	JH8/JD-1	JH8/JD-1	RGM0912	RGM0912	RGM0912	RGM09/13	RGM0916	RGM0916	RGM0916	RGM0916	RGM0916	RGM0916	RGM0916	RGM0916	RGM0916
SiO_2	60.76	62.45	63.52	62.16	62.54	61.90	62.35	62.25	62.74	62.47	62.98	63.06	62.47	62.28	63.07
Al_2O_3	16.02	16.49	17.45	17.64	17.62	16.88	18.54	18.93	18.99	18.90	19.16	18.74	16.32	16.85	18.12
FeO	3.58	3.79	1.87	2.37	2.20	2.93	1.17	1.19	0.46	0.76	0.48	0.30	3.17	2.49	0.85
CaO	0.05	0.03	0.00	0.03	0.02	0.03	0.01	0.01	0.00	0.01	0.00	0.02	0.00	0.00	0.00
Na_2O	0.18	0.23	1.51	1.61	1.52	0.11	0.08	0.18	0.02	0.00	0.07	0.08	0.31	0.26	0.17
K_2O	17.56	17.17	14.87	14.79	14.54	16.39	17.07	16.70	17.16	17.10	17.02	17.16	16.97	16.88	17.11
Total	98.15	100.17	99.23	98.61	98.43	98.24	99.21	99.25	99.37	99.24	99.71	99.37	99.24	98.76	99.32
Cations per 8 oxygen atoms															
Si	2.881	2.906	2.953	2.906	2.932	2.94	2.91	2.903	2.92	2.914	2.921	2.937	2.93	2.931	2.939
Al	0.895	0.904	0.956	0.972	0.973	0.94	1.02	1.04	1.042	1.039	1.047	1.029	0.902	0.934	0.995
Fe	0.142	0.148	0.073	0.093	0.086	0.12	0.046	0.046	0.018	0.030	0.019	0.012	0.124	0.098	0.033
Ca	0.003	0.001	0	0.002	0.001	0.00	0.001	0	0.000	0.000	0.000	0.001	0.000	0.000	0.000
Na	0.017	0.021	0.136	0.146	0.138	0.01	0.007	0.016	0.002	0.000	0.006	0.007	0.028	0.024	0.015
K	1.062	1.019	0.882	0.882	0.87	0.99	1.016	0.994	1.019	1.017	1.007	1.014	1.015	1.013	1.017
Total	5	4.999	5	5.001	5	4.999	5	4.999	5.001	5	5	5	4.999	5	4.999
An	0.23	0.14	0.00	0.15	0.10	0.15	0.05	0.05	0.00	0.05	0.00	0.10	0.00	0.00	0.00
Ab	1.53	1.99	13.36	14.17	13.69	1.01	0.71	1.61	0.18	0.00	0.62	0.71	2.70	2.29	1.49
Or	98.23	97.86	86.60	85.67	86.20	98.85	99.24	98.34	99.82	99.95	99.38	99.20	97.30	97.71	98.51

iron-enriched (see Fig. 3G) and have indistinguishable Ti, K and Na contents (Fig. 3H) compared to those reported from Raniganj rocks by Mitchell and Fareeduddin (2009). However, it should be highlighted here that composition of the Jharia amphiboles of this study contrasts, in some aspects with those from the well-characterised lamproites of Eastern Dharwar craton (southern India), Smoky Butte (Montana, U.S.A.), Leucite Hills (Wyoming, U.S.A.), West Kimberley (W. Australia), Torngat (Labrador), and Kapamba (Africa) as also noticed in case of amphiboles from Raniganj area (Mitchell and Fareeduddin, 2009).

4.6. K-feldspar

Potassium feldspar occur in minor to subordinate proportions as an anhedral groundmass phase in all the Jharia as well as Raniganj samples (Fig. 3F and G). It has a predominant orthoclase component with very minor to negligible albite and anorthite contents respectively (Table 5) and come under sanidine (Fig. 3I). Iron (FeO_T up to 3.79 wt.%) enrichment is a characteristic feature in some of the analysed grains from Jharia samples which very likely reflects the peralkaline nature of their magma (Wagner and Velde, 1986). Overall, their composition overlap with that of the K-feldspar reported from the Eastern Dharwar craton lamproites, southern India (Fig. 3I), Even though, iron enrichment has also been noticed in feldspars from Raniganj, some of them are distinctly iron-poor (<1 wt.% FeO_T) similar to those reported by Rock et al. (1992) who considered them to be feldspars typical of those found in minettes. On the other hand, alkali feldspars with high Or (>95 mol%) and Fe contents are regarded typical of sanidine occurring in lamproites (Mitchell and Bergman, 1991; Chalapathi Rao et al., 2010). No barium was detected in any of the analysed feldspars in contrast to the report of hyalophane intergrowths from the feldspars from these rocks (see Middlemost et al., 1988; Kent et al., 1998; Mitchell and Fareeduddin, 2009).

4.7. Apatite

Apatite is a ubiquitous early as well as late-stage accessory phase and at times is present up to 15 vol.% in some samples as testified by their high (>6 wt.% P_2O_5) contents (see Table 9). Three modes of paragenesis of apatite are observed: (i) acicular laths up to 1 mm in length (Fig. 3E and F), (ii) subhedral to euhedral prisms of <50 μm (Fig. 3H and I) and (iii) irregular inclusions in microphenocrystal phlogopite (Fig. 3L). Composition of apatite from Jharia and Raniganj samples is summarised in Table 6. All of them are essentially Sr-enriched with some of those from Raniganj having up to 3.39 wt.% SrO contents (Table 6). Apatites from Raniganj and Jharia of this study are indistinguishable from each other in terms of their SrO and CaO contents; however, their SrO contents are much less than those earlier reported from Raniganj samples (Fig. 3J). The SrO composition of apatites from this study is indistinguishable from those reported from Chelima lamproites, southern India, West Kimberley lamproites, western Australia and distinctly higher than those from Krishna lamproites, southern India (Fig. 3J).

4.8. Rutile

Rutile is a widespread late-stage accessory mineral in all the studied samples and occurs as (i) euhedral to subhedral crystals of 30 μm size (Fig. 2G) and (ii) as platy aggregates (Fig. 2I). Rutile is characteristically niobian (Nb_2O_5 up to 1.75 wt.%) and iron (Fe_2O_3 up to 0.73 wt.%) bearing (Table 7). Middlemost et al. (1988) and Rock et al. (1992) reported niobian-rutile from their samples, whereas Mitchell and Fareeduddin (2009) found niobium to occur below the detection limits.

Table 6
Mineral chemistry (oxide wt.%) of apatite (cores) from samples under study. Total iron is expressed as FeO.

	1	2	3	4	5	6	7	8	9	10	11
Oxide (wt.%)	JH8/BH2	JH8/BH2	JH8/BH2	JH8/BH2	JH8/BH2	RGM09/16	RGM/09/16	RGM09/8	RGM09/8	RGM 09/8	RGM 09/8
CaO	52.96	53.68	54.00	54.46	53.94	52.00	51.93	51.94	52.06	53.59	53.14
Na_2O	0.03	0.06	0.07	0.07	0.03	0.11	0.18	0.15	0.15	0.04	0.03
SrO	1.37	1.35	1.60	1.40	1.30	3.39	3.30	3.15	3.14	1.61	2.12
FeO	0.34	0.16	0.50	0.35	0.38	0.27	0.40	0.48	0.28	0.59	0.24
La_2O_3	0.24	0.25	0.22	0.24	0.25	0.30	0.27	0.32	0.24	0.08	0.36
Ce_2O_3	0.49	0.53	0.68	0.55	0.57	0.81	0.83	0.87	0.69	0.17	0.95
Pr_2O_3	0.03	0.03	0.01	0.08	0.05	0.09	0.04	0.10	0.00	0.03	0.08
Nd_2O_3	0.24	0.25	0.26	0.22	0.25	0.38	0.56	0.37	0.34	0.19	0.35
ThO2	0.00	0.01	0.00	0.00	0.04	0.00	0.01	0.00	0.01	0.01	0.05
P_2O_5	42.71	41.39	42.07	42.21	41.83	41.38	41.97	41.63	41.15	41.49	41.39
SiO_2	0.74	1.60	0.90	0.88	0.90	0.76	0.63	0.81	0.81	1.40	1.25
Total	99.13	99.33	100.32	100.44	99.53	99.49	100.11	99.80	98.87	99.20	99.98
Cations based on 25 oxygen atoms											
Ca	9.440	9.594	9.594	9.647	9.642	9.414	9.331	9.358	9.461	9.586	9.523
Na	0.010	0.020	0.024	0.021	0.010	0.034	0.058	0.047	0.049	0.014	0.010
Sr	0.133	0.130	0.154	0.134	0.125	0.332	0.321	0.307	0.309	0.156	0.206
Fe	0.048	0.022	0.070	0.048	0.053	0.037	0.056	0.068	0.040	0.082	0.033
La	0.015	0.016	0.013	0.014	0.015	0.019	0.017	0.020	0.015	0.005	0.022
Ce	0.030	0.032	0.041	0.033	0.035	0.050	0.051	0.053	0.043	0.010	0.058
Pr	0.002	0.002	0.000	0.005	0.003	0.006	0.003	0.006	0.000	0.002	0.005
Nd	0.014	0.015	0.015	0.013	0.015	0.023	0.033	0.022	0.020	0.011	0.021
Th	0.000	0.000	0.000	0.000	0.002	0.000	0.000	0.000	0.000	0.000	0.000
Pr	6.059	5.845	5.906	5.909	5.908	5.919	5.959	5.927	5.909	5.863	5.862
Si	0.124	0.267	0.149	0.145	0.150	0.128	0.106	0.137	0.138	0.234	0.209
Total	15.874	15.943	15.968	15.969	15.959	15.834	15.933	15.945	15.984	15.963	15.741

4.9. Carbonate

Carbonate is an important groundmass constituent in the studied samples (Fig. 2C and D) and also occurs as a pseudomorphous phase after olivine (Fig. 2A and B). Some samples contain very high carbonate contents as also attested by their loss on ignition (LOI) contents of up to 22 wt.% (Table 9). Ferroan dolomite is the sole carbonate variety encountered this study (Table 8); however, ankerite, witherite, strontianite and breunnerite have been reported from the Damodar valley ultrapotassic rocks (Rock et al., 1992; Kent et al., 1998; Mitchell and Fareeduddin, 2009).

4.10. Ilmenite

Prismatic grains of groundmass ilmenite are noticed in a few samples. Compositionally they are magnesian–mangoan ilmenites (MgO: 1.21–1.87 wt.%; MnO: 0.63–0.80 wt.%; Table 8) which are impoverished in magnesia compared to those (MgO up to 6.27 wt.%)

Table 7
Mineral chemistry (oxide wt.%) of rutile in the samples under study. Total iron is expressed as Fe_2O_3.

	1	2	3	4	5	6
Oxide wt.%	RGM09/8	RGM09/8	RGM09/8	JH8/BH2	JH8/BH2	JH8/BH2
TiO_2	97.02	95.73	97.49	97.78	96.95	99.05
Fe_2O_3	0.57	0.59	0.42	0.73	0.70	0.28
Nb_2O_5	0.85	1.74	1.01	1.16	0.84	0.62
Ta_2O_5	0.02	0.05	0.01	0.09	0.00	0.06
MnO	0.03	0.02	0.02	0.02	0.03	0.05
Total	98.49	98.14	98.95	99.78	98.53	100.05

Table 8
Mineral chemistry (oxide wt.%) of carbonate, ilmenite and chlorite from the samples under study.

	Carbonate				Ilmenite					Chlorite		
Oxide wt.%	RGM09/08	RGM09/08	RGM09/10	JH8/7B	JH8/BH2	JH8/BH2	JH8/BH2	JH8/BH2	JH8/BH2	RGM09/8	RGM09/8	JH8/7B
SiO_2	0.29	0.04	0.76	0.26	–	–	–	–	–	28.50	28.02	31.32
Al_2O_3	0.02	0.00	0.05	1.13	–	–	–	–	–	15.67	15.62	13.14
TiO_2	0.70	0.01	0.07	0.05	51.74	51.77	51.89	51.72	53.21	0.01	0.04	4.70
FeO	5.48	7.25	45.79	27.91	46.47	46.08	47.06	47.15	44.79	29.11	29.61	16.91
MnO	0.51	0.24	0.27	1.16	0.64	0.66	0.73	0.80	0.63	0.01	0.02	0.06
MgO	18.58	13.54	12.15	13.74	1.87	1.75	1.21	1.58	1.73	13.64	13.29	18.42
CaO	30.95	33.80	29.25	15.76	–	–	–	–	–	0.26	0.22	0.32
Total	56.53	54.96	54.96	54.96	100.72	100.26	100.89	101.25	100.36	87.20	86.82	84.87

Table 9
Major element composition (oxide wt.%) and CIPW norms of the samples under study. Sample details (co-ordinates, location, nature and classification as per TAS plot) are also provided.

Sample	RGM-09/1	RGM-09/2	RGM-09/3	RGM-09/4	RGM-09/5	RGM-09/6	RGM-09/8	RGM-09/10	RGM-09/12	RGM-09/13	RGM-09/14
Rock type	B, subal	B, subal	TB, pot	FOI, mnp	FOI, mnp	FOI, mnp	TEP, mnp	FOI, mnp	PHT	B, subal	TB, pot
Latitude	23°38′76″N				23°42′55″N			23°35′65″N	23°43′80″N	23°46′33″N	
Longitude	87°03′97″E				87°02′98″E			87°02′28″E	86°43′86″E	86°43′86″E	
Basin	Raniganj				Raniganj			Raniganj	Raniganj	Raniganj	
Location	JK Nagar */underground mine				Nigah underground mine			Kalidaspur underground mine	Bhanra West, underground mine	Lakimata mine	
Nature of sample	Underground mine sample				Underground mine sample			Underground mine sample	Underground mine sample	Underground mine sample	
SiO_2	45.57	44.47	39.94	33.56	33.6	33.89	36.46	29.27	44.52	38.56	43.93
TiO_2	5.931	5.834	6.314	5.866	4.527	4.665	6.449	6.299	6.453	4.726	8.453
Al_2O_3	6.43	6.76	7.09	6.79	6.36	7.06	6.61	5.67	8.25	4.98	7.27
$Fe_2O_3^T$	10.43	10.11	10.29	11.26	10.25	8.99	10.3	12.12	8.04	10.28	12.11
MnO	0.096	0.078	0.108	0.128	0.199	0.088	0.104	0.114	0.101	0.132	0.139
MgO	10.42	9.67	10.29	9.26	9.79	7.15	10.64	7.51	8.13	11.66	5.61
CaO	5.95	7.53	8.03	9.62	13.22	14.69	10.32	13.66	3.9	8.77	3.88
Na_2O	0.11	0.11	0.1	0.13	0.13	0.16	0.07	0.53	0.76	0.09	0.09
K_2O	3.82	3.77	4.46	4.62	1.34	0.95	3.32	2.7	6.66	2.76	6.25
P_2O_5	1.51	2.6	1.95	2.37	6.01	6.67	2.34	6.23	2.33	3.32	2.58
LOI	8.34	8.71	10.05	14.77	12.07	13.2	12.06	13.54	8.11	11.8	7.51
Total	98.61	99.64	98.62	98.37	97.49	97.5	98.67	97.64	97.27	97.07	97.81
CIPW normative minerals											
Q	8.518	8.406	–	–	1.838	8.157	–	–	2.086	2.095	11.634
Or	25.258	24.732	30.033	14.542	9.372	6.719	22.882	19.206	44.458	19.325	41.332
Ab	1.041	1.032	0.965	–	1.303	1.625	0.694	4.713	6.048	0.905	0.855
An	6.454	7.57	6.523	5.203	15.159	18.844	9.23	6.16	–	5.96	1.089
Lc	–	–	–	14.5	–	–	–	–	–	–	–
Ne	–	–	–	0.72	–	–	–	0.371	–	–	–
Ac	–	–	–	–	–	–	–	–	1.068	–	–
Di	12.265	11.88	19.064	26.847	12.82	12.949	25.683	21.094	2.94	15.768	1.238
Hy	27.365	24.909	18.938	–	30.791	20.738	9.239	–	21.51	33.506	15.063
Ol	–	–	2.051	15.049	–	–	9.004	13.452	–	–	–
Mt	2.581	2.482	3.613	3.013	2.09	1.856	2.656	3.226	–	2.694	4.028
He	–	–	–	–	–	–	–	–	1.806	–	0.102
Il	12.605	12.303	13.666	13.482	10.174	10.61	14.287	14.402	13.364	10.635	17.968
Ap	3.913	6.686	5.148	6.645	16.45	18.503	6.323	17.374	6.098	9.112	6.689
Tn	–	–	–	–	–	–	–	–	0.6206	–	–
Ks	–	–	–	–	–	–	–	–	–	–	–
Cs	–	–	–	–	–	–	–	–	–	–	–
Mg#	70.019	69.097	71.556	65.781	68.227	64.134	70.715	59.156	72.484	72.612	53.82
K/Na	38.86	38.35	49.90	39.76	11.53	6.64	53.07	5.70	9.81	34.31	77.70
K/Al	0.93	0.87	0.99	1.07	0.33	0.21	0.79	0.75	1.27	0.87	1.37

Abbreviations: $Fe_2O_3^T$ = total iron expressed as Fe_2O_3; Mg# = 100 $Mg^{2+}/(Mg^{2+} + Fe^{2+})$, atomic; Rock-types are presented according to total alkalis versus silica diagram (Le Bas, 2000) and CIPW norms are on an anhydrous 100% adjusted basis and using Fe_2O_3/FeO ratio after Middlemost (1989), using the SINCLAS computer program (Verma et al., 2002). B = basalt; FOI = foidite; TB = trachybasalt; TEP = tephriphonolite; PHT = phonolite; PIC = picrite; BSN = basanite.

reported by Mitchell and Fareeduddin (2009) from Raniganj samples.

4.11. Others

Chlorite occurs predominantly as a pseudomorphous phase after primary ferromagnesian minerals (Table 8). Quartz also occurs as a minor accessory in many of the samples.

5. Geochemistry

The major (along with their CIPW norms) and trace element data of the analysed samples is presented in Tables 9 and 10 respectively. All the Raniganj as well as Jharia samples of this study are weakly to strongly ultrabasic (SiO_2: 29.27–45.93 wt.%) and have variable, but nevertheless high, MgO contents ranging from 5.61 to 18.18 wt.% (Table 9). Their alumina and iron display a relatively tight range (Al_2O_3: 4.03–8.23 wt.% and $Fe_2O_3^T$: 7.75–12.51 wt.%). High TiO_2 (4.52–8.70 wt.%) and P_2O_5 (1.53–6.23 wt.%) contents are a characteristic feature of these rocks highlighting the dominance of modal rutile and apatite respectively. All of them are strikingly impoverished in sodium ($Na_2O < 0.73$ wt.%) owing to the paucity of sodium-bearing feldspar and ferromagnesian minerals. Studied samples are highly enriched in potassium (K_2O up to 6.66 wt.%), strongly ultrapotassic (molar K/Na: 5–110), many of them are also perpotassic (molar K/Al: 1.07–1.86) as well as peralkaline (molar K + Na/Al: 1.01–2.0; Table 9). Varying CaO contents (3.09–14.69 wt.%) reflect the proportion of the carbonate mineral assemblages whereas high loss on ignition contents (LOI: 7.51–22.99 wt.%) illustrate the hydrous and volatile mineralogy of the rocks. Their undersaturated, alkaline as well as peralkaline nature is further attested by the appearance of normative olivine, nepheline, leucite and acmite respectively in many of these rocks (Table 9). The rest of the samples are slightly quartz normative owing to the modal quartz in them. All the samples have high contents of normative ilmenite (10.15–19.20) and apatite (3.9–18.5) reflecting the high proportion of modal rutile/ spinel (iron oxides) and apatite respectively (Table 9). Molar Mg# [$(Mg/Mg + Fe^{2+}) \times 100$] for many of the samples is > 70 and imply only a small degree of fractionation. For those with relatively low Mg# (53–59) normative quartz is invariably present (Table 9) thereby implying some role of differentiation processes. High concentration of

RGM-09/16	JH8/7B	JH08/JD-1	JH8/BH1	JH8/BH2	JH8/BH12	JH8/BH13	BM-10/2	BM-10/3	BM-10/4
TEP, mnp	TB, pot	PIC	BSN, mnp	BSN, mnp	FOI, mnp	FOI, mnp	TEP, mnp	BSN, mnp	BSN, mnp
23°45′85″N	23°41′39″N	23°48′51″N	23°39′30″N to 23°42′55″N				23°41′10″N	23°41′15″N	23°41′12″N
86°33′72″E	85°19′82″E	86°15′43″E	86°19′15″E to 86°12′30″E				86°21′33″E	86°21′33″E	86°21′34″E
Raniganj	Karanpura	Jharia	Jharia				Jharia	Jharia	Jharia
Shyampur 'B'	Sayal, near Damodar River	Jogidih seam I	Parbatpura coal block				Parbatapura coal block		
Underground mine sample	Surface sample	underground mine sample	underground mine sample				Bore hole sample		
41.79	45.93	31.5	33.31	37.74	32.02	27.83	39.34	37.05	36.32
7.505	6.943	5.539	7.063	4.724	5.137	5.744	8.707	6.971	6.089
6.98	7.25	5.05	4.74	7.47	7.8	4.08	6.37	4.48	4.03
12.51	7.75	9.13	10.83	9.74	8.77	11.21	10.66	10.37	10.51
0.13	0.059	0.127	0.142	0.14	0.125	0.145	0.134	0.14	0.158
7.63	8.17	10.56	13.21	12.27	10.43	18.18	6.03	13.75	16.74
3.09	6.58	14.69	5.46	8.11	8.13	4.21	5.52	5.01	4.32
0.08	0.17	0.12	0.12	1.2	0.17	0.09	0.06	0.39	0.19
5.77	4.99	2	3.8	5.27	5.83	3.75	5.94	4.75	4.77
2.06	2.74	6.03	2.01	2.46	2.84	1.13	2.62	1.71	1.53
10.56	8.37	14.35	18.22	8.29	15.19	22.99	12.74	13.42	13.7
98.09	98.95	99.08	98.9	97.41	96.44	99.36	98.14	98.04	98.35
7.202	10.62	–	–	–	–	–	6.319	–	–
39.394	32.775	14.083	28.153	20.495	7.246	–	41.138	29.187	26.266
0.778	1.599	1.21	1.269	–	–	–	–	–	–
1.902	4.758	8.735	1.469	–	4.096	–	–	–	–
–	–	–	–	11.566	27.853	23.04	–	–	–
–	–	–	–	5.568	0.967	0.078	–	–	–
–	–	–	–	1.068	–	0.76	0.529	3.466	1.692
0.204	6.728	24.569	12.57	21.549	17.974	8.408	8.939	12.76	10.735
24.083	19.5	11.653	12.906	–	–	–	13.623	17.461	14.53
–	–	8.697	17.972	20.286	18.228	44.631	–	13.328	24.766
4.454	–	1.874	3.002	2.862	3.355	2.906	–	2.076	1.927
–	1.831	–	–	–	–	–	2.497	–	–
16.468	13.028	12.534	16.819	10.154	12.112	14.466	19.201	15.799	13.806
5.514	7.055	16.644	5.838	6.45	8.167	3.471	7.18	4.726	4.231
–	2.1066	–	–	–	–	–	0.465	–	–
–	–	–	–	–	–	–	0.106	1.194	2.046
–	–	–	–	–	–	2.238	–	–	–
60.544	72.62	72.226	74.034	76.014	74.951	79.127	58.73	76.936	78.827
80.70	32.84	35.43	4.91	38.37	46.62	18.65	110.77	13.63	28.09
1.30	1.08	1.26	1.11	1.17	1.44	0.62	1.46	1.66	1.86

compatible trace elements (e.g., Cr: 270–1140 ppm; Ni: 20–580 ppm; V: 116–297 ppm; Co:35–92; Sc:16–40 ppm; Table 10) once again highlights the small-degree of fractionation undergone by the original magma(s). On the other hand, several incompatible trace elements show far wider range in their abundances (Rb: 28–164 ppm; Sr: 1740–6142 ppm; Ba: 1869–8805 ppm; Table 10).

Variation diagrams involving major oxides versus MgO of the samples illustrate moderate to conspicuous increase in SiO_2, Al_2O_3, $Fe_2O_3^*$, TiO_2, CaO, K_2O and P_2O_5 with decreasing MgO (Fig. 4A–G) illustrating their compatibility in fractionating phases and highlights the role of differentiation and fractional crystallisation. Some of the earlier studied Jharia ultrapotassic rock samples (Srivastava et al., 2009) are also plotted for a comparison throughout. The coefficient of correlation (R), inferred for trendlines depicted, vary from 0.82 to 0.36 (Fig. 4A–G). Samples from Jharia and Raniganj display an overlapping geochemical character in all these plots. Loss on ignition (LOI) of the samples correlates positively with MgO contents implying the role of Mg-bearing phases such as carbonate (Fig. 4H); this is further illustrated by the good correlation displayed between CaO and LOI (Fig. 4I). Transitional element e.g., Ni (Fig. 4J) and Cr (Fig. 4K) content decrease with a concomitant decrease in their respective MgO thereby suggesting their compatibility in fractionating phases such as olivine and to a lesser extent that of phlogopite. High degree inter-element correlations between high field strength elements (HFSE) such as Zr–Hf (Fig. 4L) and Nb–Ta (Fig. 4M) and large ion lithophile (LILE) elements such as K–Rb (Fig. 4N) demonstrate the limited influence of post-magmatic secondary and. or hydrothermal alterations on the samples under study. On the other hand, a lack of correlation between Zr and La (Fig. 4O) and Zr and Sr (Fig. 4P) suggests that HFSE (viz., La and Zr) and LILE (such as Sr) are incompatible in the fractionating phases.

In two of the robust and updated discriminant plots (MgO vs SiO_2 wt.% and TiO_2 versus Al_2O_3 wt.%; not shown) involving major oxide data sets for classification of alkaline potassic rocks, all the samples of this study show firm affinities towards ultramafic lamprophyres and lamproites respectively as also displayed by some of the Jharia samples earlier studied by us (see Fig. 4A and B in Srivastava et al., 2009). Th and Co contents in bulk-rocks have been recently shown to be of petrogenetic importance in deciphering the broad parental magma types (Hastie et al., 2007) and all the ultrapotassic rock samples of this

Table 10
Trace element (ppm) concentration of samples under study.

Trace elements	RGM-09/1	RGM-09/2	RGM-09/3	RGM-09/4	RGM-09/5	RGM-09/6	RGM-09/8	RGM-09/10	RGM-09/12	RGM-09/13	RGM-09/14	TRGM-09/16	JH8/7B	JH08/JD-1	JH8/BH1	JH8/BH2	JH8/BH12	JH8/BH13	BM-10/2	BM-10/3	BM-10/4
Sc	18	20	19	19	40	39	28	34	19	25	18	18	17	29	19	22	22	18	18	16	16
V	207	170	209	181	116	134	186	211	179	174	264	297	269	125	197	203	193	196	243	196	177
Ba	2515	2501	2720	3022	2429	2101	2464	1928	8805	2624	2604	2826	4269	2360	2237	4419	4741	2390	1869	4912	2712
Sr	1375	2329	1405	1879	5185	6142	1257	4768	4792	5173	1456	1740	2584	6852	2030	2873	2714	2067	2556	2366	1967
Y	32	49	35	39	148	174	38	136	32	81	49	47	27	117	44	40	47	36	61	42	38
Zr	1237	1045	1192	1061	360	599	1115	862	1027	799	729	855	1314	775	1320	688	470	1166	647	1173	1019
Cr	1140	340	440	420	330	390	530	270	470	440	280	310	770	390	270	1070	800	450	470	290	370
Co	92	39	58	52	51	48	67	51	39	47	52	48	34	41	35	51	45	65	34	47	70
Ni	580	460	420	450	370	300	430	330	330	490	170	240	220	310	60	220	220	280	20	160	360
Cu	50	40	60	50	50	40	50	50	30	50	100	100	180	80	10	60	40	30	30	20	20
Zn	130	150	120	120	140	120	110	180	120	160	230	180	170	120	130	120	130	160	130	120	120
Ga	19	25	20	23	38	33	26	40	22	27	24	27	18	18	13	18	18	16	27	21	19
Rb	113	66	123	77	30	28	115	56	127	56	90	97	160	33	76	141	125	141	156	160	164
Nb	207	99	190	121	146	175	244	121	89	87	109	116	30	91	94	101	79	96	149	185	159
Cs	0.6	<0.5	0.5	0.6	0.5	<0.5	0.7	1.2	<0.5	0.6	<0.5	<0.5	<0.5	1.3	<0.5	14	1	1	<0.5	<0.5	0.8
Hf	33.7	26	32.7	22.7	12.4	20.1	28.4	23	26.9	22.2	15.8	18.2	30.5	22.6	19.5	15.6	8.5	33.8	11.4	27.7	24.5
Ta	9.4	4.5	9.7	6.4	4.9	5.1	12.2	3.8	4.1	3.8	6.7	6.6	1.8	5.9	7.8	8	7.8	7.8	11.9	12.1	10.4
Pb	33	49	35	29	158	158	35	98	56	58	49	39	52	16	15	18	6	21	41	34	30
Th	24.8	21.2	25.4	20.7	105	112	54.8	62.4	19.5	29.8	21.6	21.8	9.5	51.9	19.4	26.5	25.2	23.3	44.2	26.7	25.7
U	5.6	4.9	6	5.1	11.2	9.9	10.4	10.7	4.3	7.8	5.7	5.2	3.7	10.2	1.1	4.9	3.9	2.1	6.7	4.3	4.8
La	270	293	291	263	1120	1240	468	811	313	396	254	230	198	680	187	268	332	199	323	352	330
Ce	552	626	623	565	2160	2390	1050	1660	679	841	532	481	490	1420	373	546	683	413	619	683	652
Pr	68.1	74.2	68.6	66	217	291	118	182	79	98.8	64.4	57.9	58	189	40.2	60	87.9	45.1	74.7	81.7	78.4
Nd	244	286	252	256	850	1070	419	748	290	400	257	231	178	666	133	188	248	146	259	281	269
Sm	32.2	43.2	33.6	37.6	124	155	50	122	37	62.9	41.9	37.1	33.9	105	25.3	36.2	42.7	28.5	41.6	43	39.2
Eu	7.61	10.5	7.91	9.17	30.6	37.9	10.4	29.7	9.32	15.7	10.9	9.78	7.23	26.9	6.66	9.1	10.7	7.55	11	10.6	9.48
Gd	17.6	25.9	18	22.4	79.5	88	24.7	74.5	19.1	39.1	25.8	22.8	16.9	61.6	15	21	24.9	16.8	28	24.7	21.6
Tb	1.9	2.7	2	2.1	8	9.7	2.3	7.8	1.8	4.2	2.8	2.6	1.6	7.1	1.7	2.3	2.7	1.9	3.6	2.8	2.4
Dy	8.4	11.5	9	9.4	34.6	43.3	9.6	33.3	7.2	18.8	12	11.1	6.6	29.3	7.5	9.6	11.2	8.1	16.9	11.9	10.7
Ho	1.3	1.8	1.4	1.4	5.3	6.6	1.4	4.9	1	2.9	1.8	1.7	1	4.5	1.2	1.4	1.7	1.3	2.6	1.8	1.7
Er	2.9	3.8	3	3.2	12	14.8	2.9	11.1	2.3	6.7	4	3.9	2.4	11	2.9	3.4	4.3	3.3	6.2	4.4	4.3
Tm	0.35	0.45	0.36	0.4	1.41	1.79	0.34	1.3	0.28	0.8	0.49	0.48	0.29	0.98	0.36	0.41	0.5	0.43	0.67	0.47	0.5
Yb	1.9	2.6	2	2.2	7.8	10	1.9	7.2	1.7	4.4	2.6	2.7	1.5	6.1	1.9	2	2.5	2.3	3.5	2.4	2.7
Lu	0.27	0.35	0.29	0.3	1.11	1.39	0.25	0.98	0.25	0.6	0.35	0.38	0.18	0.69	0.22	0.24	0.31	0.32	0.45	0.32	0.36

study plot in the high-K-calc-alkaline and shoshonitic fields (Fig. 5) and are distinct from the Eastern Dharwar craton Mesoproterozoic lamproites (also shown for comparison in Fig. 5) in having higher Th and lower Co contents. The total REE abundances of the Jharia (1208–5359 ppm) samples of this study are relatively higher than those from Raniganj (795–3328 ppm). The chondrite-normalised rare earth element distribution patterns (Fig. 6A) of all the studied samples are steep and show conspicuous light rare element (LREE) enrichment (800–2000× chondrite) compared to their heavy rare earth elements (10–40× chondrite). The patterns for Raniganj as well as Jharia samples are parallel and overall indistinguishable from each other. Such steep chondrite-normalised REE patterns are considered to be characteristic of potassic–ultrapotassic rocks (e.g. Tainton and McKenzie, 1994; Le Roex et al., 2003). The primitive-mantle normalised multi-element distribution patterns for the Jharia and Raniganj samples are provided in Fig. 6B and C respectively. All of them are highly enriched (20–1000×) over the primitive-mantle and reveal the following aspects: (i) Jharia samples of this study display varying negative anomalies at Nb–Ta, K, Pb and Zr–Hf; (ii) the magnitude of such anomalies in samples earlier studied by us (Srivastava et al., 2009) from the Jharia area is relatively less and all of them collectively have a positive Pb anomaly; (iii) the Raniganj samples, on the other hand, are free from troughs at Nb–Ta and are characterised by negative K, Pb and Sr anomalies and (iv) none of the samples have Eu anomaly negating plagioclase fractionation (either by crystal fractionation or upper crust contamination) during the evolution of their magmas. The anomalies in the multi-element normalised patterns are generally attributed either to (i) residual phases in the source regions or (ii) reflect the hydrothermal

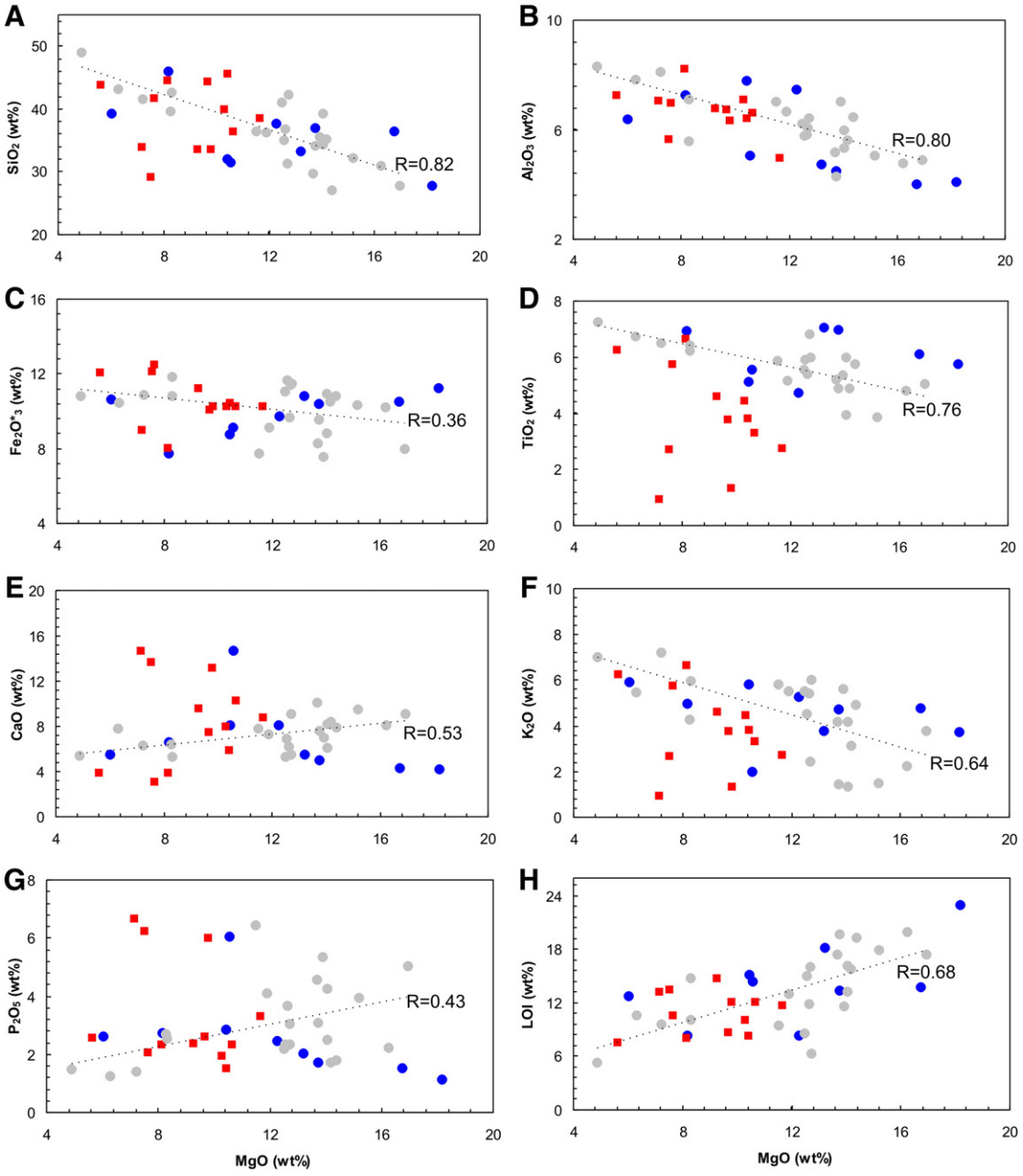

Fig. 4. Bi-variate plots involving MgO (wt.%) versus (A) SiO_2 (wt.%), (B) Al_2O_3 (wt.%), (C) Fe_2O_3* (wt.%) (D) TiO_2 (wt.%), (E) CaO (wt.%), (F) K_2O (wt.%), (G) P_2O_5 (wt.%) and (H) LOI (wt.%). Bi-variate plots of (I) CaO (wt.%) versus LOI (wt.%), (J) MgO (wt.%) vs Ni (ppm), (K) MgO (wt.%) vs Cr (ppm), (L) Zr (ppm) vs Hf (ppm), (M) Nb (ppm) vs Ta (ppm), (N) K (ppm) vs Rb (ppm), (O) Zr (ppm) vs La (ppm) and Zr (ppm) vs Sr (ppm). Symbols for Jharia and Raniganj samples remain the same as in Fig. 3A and the gray circle represents data for Jharia ultrapotassic rocks reported by Srivastava et al. (2009). Dotted lines in each panel represent trend lines for all the data sets presented and their coefficient of correlation (R) is also provided.

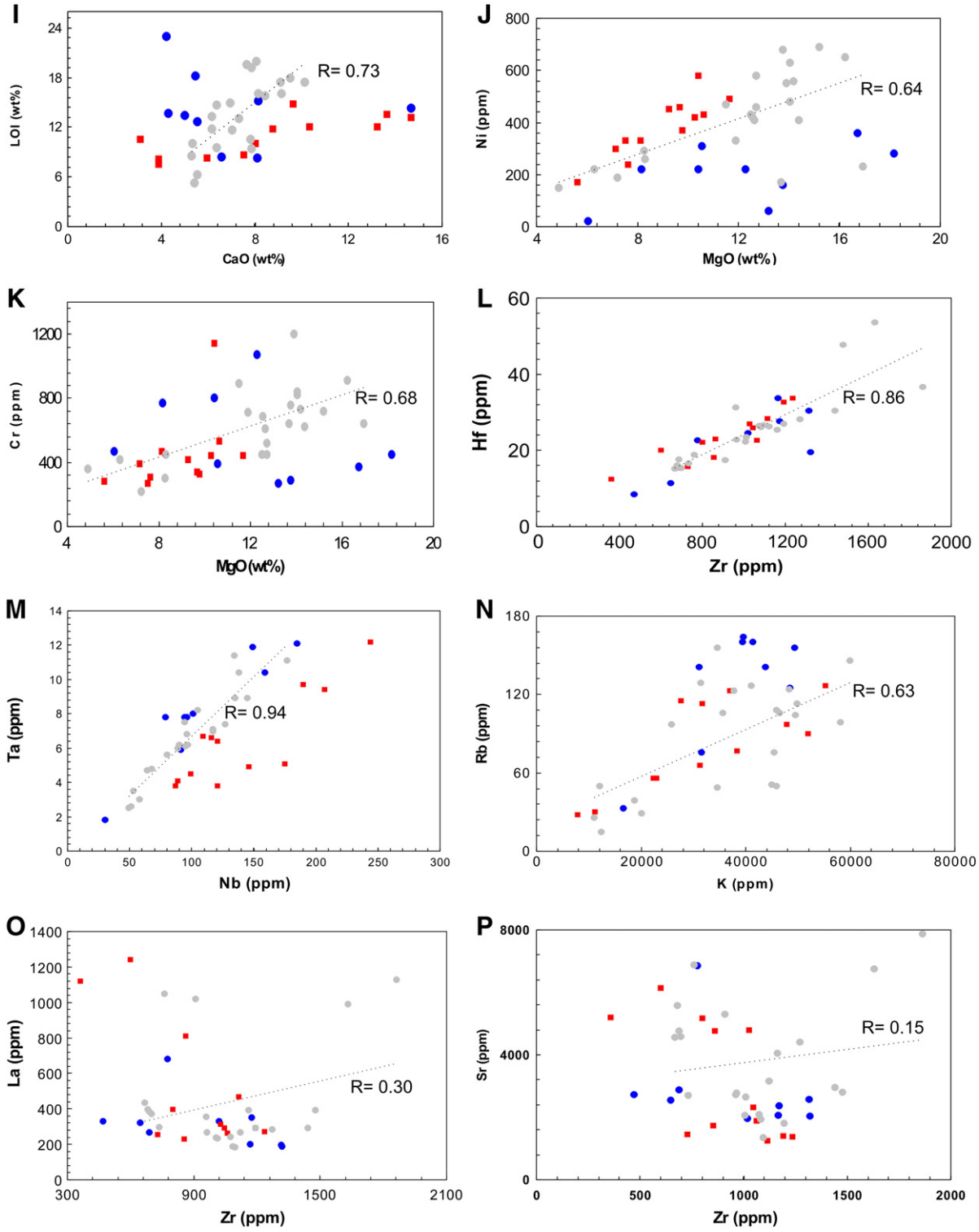

Fig. 4 (*continued*).

and/or secondary alteration subjected to by the samples or even (iii) related to fractionating phases (see Gibson et al., 1995; Becker and Le Roex, 2006; Coe et al., 2008). As samples with high and low Mg numbers contain similar patterns we infer fractionation not to be responsible for their origin. Because post-magmatic hydrothermal alteration is considered not to have exercised a significant influence (above) we attribute the anomalies in multi-element plots to be source-related.

Both the $^{87}Sr/^{86}Sr_m$ and $^{143}Nd/^{144}Nd_m$ ratios of three Jharia and one Raniganj sample are corrected to an emplacement age of 114 Ma (Ghatak and Basu, 2013) and their initial ratios as well as depleted mantle (T_{DM}) model ages are presented in Table 11. Initial $^{87}Sr/^{86}Sr$ ratios in three samples from Jharia show little variation and range from 0.704637 to 0.705247. However, one sample from Raniganj is more radiogenic and displays a higher value of 0.712919. The $^{143}Nd/^{144}Nd$ initial ratios of the Jharia samples are also tightly clustered (0.512316 to 0.512372)

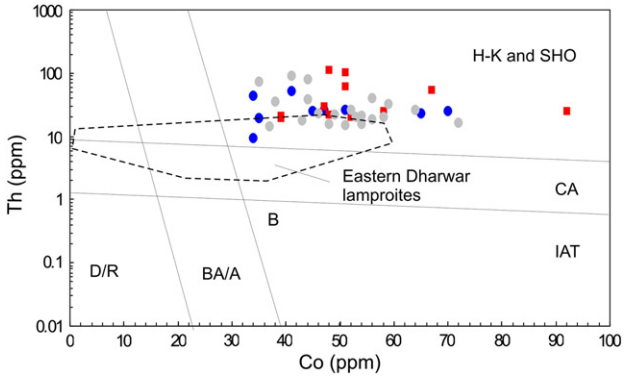

Fig. 5. Co (ppm) vs Th (ppm) discrimination plot (after Hastie et al. 2007) for the samples under study. Gray circle represents data for Jharia ultrapotassic rocks reported earlier by Srivastava et al. (2009) and the symbols remain the same as in Fig. 4. The field of Eastern Dharwar craton lamproites is from Chalapathi Rao et al. (2004, 2010) and Paul et al. (2007). Abbreviations: D/R = dacite and rhyolite; BA/A = basaltic andesite and andesite; B = basalt; IAT = island arc tholeiites; CA = calc-alkaline; H-K and SHO = high-K calc-alkaline and shoshonitic.

with the Raniganj sample (RGM09/8) displaying a slightly lower value of 0.512268. As this sample shows relatively low SiO_2 (36.46 wt.%) and Na_2O (0.07 wt.%) and high #Mg contents (70.71) (Table 9) we negate the role of alteration or crustal contamination in influencing the isotopic composition and infer the distinct Sr and Nd initial ratio to be a source-related and of significant to its petrogenesis.

In the ε_{Ndi} versus $^{87}Sr/^{86}Sr_i$ space (Fig. 7), the Jharia and Raniganj samples of this study plot in the 'enriched' quadrant implying derivation of the source magmas dominantly from melt source regions with lower time-integrated Sm/Nd ratios than Bulk Silicate Earth. Isotopically they are very different from those of (i) Group I kimberlites of southern Africa, (ii) Mesoproterozoic Group I kimberlites from Eastern Dharwar Craton, southern India, (iii) southern African and central Indian orangeites which have higher $^{87}Sr/^{86}Sr_i$ and lower ε_{Ndi} and (iv) primitive Kerguelen plume component (Fig. 7). Their ε_{Ndi} values range from −2.3 to −3.4 and are indistinguishable from those reported earlier for ultrapotassic rocks from the Damodar valley by Middlemost et al. (1988), Rock et al. (1992), Kumar et al. (2003) and Ghatak and Basu (2013) [Fig. 7] and are identical to those of the pristine Kerguelen mantle plume derived basalts (Fig. 7). Their $^{87}Sr/^{87}Sr_i$ is similar to those of the Mesoproterozoic lamproites from eastern Dharwar craton, Labrador and Greenland but have higher ε_{Ndi} values (Fig. 7). Note that Raniganj sample of this study together with a sample from Jharia area reported by Middlemost et al. (1988), owing to their high radiogenic strontium, are plotted differently but their ε_{Ndi} values are all similar to those from unradiogenic ultrapotassic rocks from the Damodar valley (Fig. 7). The depleted mantle Nd model age ($T_{DM;}$ see Table 4) of the Raniganj sample is ~1426 Ma and is clearly older by ~500 Ma than those from the Jharia samples (T_{DM} = 883–963 Ma) thereby implying a distinct temporal difference in their source enrichment.

6. Discussion and petrogenesis

The samples under study have broadly similar mineralogy but variable texture (porphyritic, glomeroporphyritic, interstitial, flow etc.) and yet are confined to a single compositional group. This is a characteristic feature found in some varieties of alkaline, calc-alkaline and ultramafic lamprophyres (Rock, 1984; Srivastava and Chalapathi Rao, 2007; Bratzdrum et al., 2009) and rarely in lamproites (Chalapathi Rao et al., 2010). Mica compositions and their evolutionary trends are generally considered as reliable petrogenetic indicators (Mitchell, 1995; Brod et al., 2001; Matchan et al., 2009) but are found to be equivocal in this study and suggest an overall affinity to those of lamproites, rarely to those of orangeites, and very rarely to those of calc-alkaline and ultramafic lamprophyres and none towards kimberlite. Compositional variation displayed by groundmass spinel is similar to that reported from those archetypal (Group-I) kimberlites, orangeites and lamproites. On the other hand, the clinopyroxene composition shows unmistakable lamproitic affinities. Amphibole compositions in the samples are extremely iron-enriched and in terms of their K, Na and Ti composition are very different from those recorded in lamproites from the Eastern Dharwar craton, southern India as well as global lamproite compositions e.g., Smoky Butte, Leucite Hills, West Kimberley and Kapamba. Iron-rich sanidine in these rocks is similar to such sanidine compositions from many lamproites. Rutile and carbonate, which are supposedly non-characteristic of lamproites (Mitchell and Bergman, 1991) are, in fact, ubiquitous in the present samples. Likewise, K-rich titanate (corresponding to the composition of potassium triskaidecatitanate) recorded recently from one of the samples of this study (JH8-BH2; Chalapathi Rao et al., 2013b) is considered by the IUGS to be a characteristic mineral of the Group-II kimberlites (orangeites; see Le Maitre, 2002). Thus, detailed petrographic and mineral chemistry studies carried out reveal that this sample set cannot be characterised sensu stricto by deploying the existing mineral-genetic classification schemes in vogue (e.g., Woolley et al., 1996; Le Maitre, 2002) for the nomenclature of alkaline rocks—a conclusion also reached by several previous workers (above). Therefore, the recent nomenclature of Raniganj ultrapotassic rocks as peralkaline lamproites *var*. Damodar (Mitchell and Fareeduddin, 2009) cannot be extrapolated to all such rocks in the Damodar Valley, including to occurrences from Raniganj area, as some of them are not peralkaline either in terms of their bulk geochemistry or even mineralogy.

The robustness of the mineral chemistry as a sole criterion in classifying alkaline potassic–ultrapotassic rocks (Mitchell, 1995) has also been questioned by Taylor and Kingdom (1999) who stressed the need to place reliance on appropriate trace element and isotopic discriminators. On the other hand, Srivastava et al. (2009) inferred these rocks to display magmatic traits of aillikite (a variety of carbonate-rich ultramafic lamprophyre consisting of various phenocrysts including olivine, diopside, pyroxene, amphibole, and phlogopite in a matrix of similar mineralogy with minor perovskite; Le Maitre, 2002). This inference was based on (i) extremely low concentrations of sodium, silica and alumina (uncharacteristic of kimberlites, lamproites and orangeites), enrichment in potassium, titanium and phosphorous in some of the Jharia ultrapotassic rock samples and (ii) their strong geochemical similarity to ultramafic lamprophyres from Aillik Bay area, Labrador (see Malpas et al., 1986; Tappe et al., 2004). Although aillikites sensu stricto lack K-feldspar, are not peralkaline and contain aluminous mica and pyroxene (see Tappe et al., 2005; Mitchell and Fareeduddin, 2009) we consider that the close bulk-compositional similarity of these rocks to those of aillikites from Labrador, in conjunction to our previously studied samples from the Jharia area (see Srivastava et al., 2009) are too significant to be overlooked. Interestingly, rocks with similar bulk geochemical and petrographic characteristics to lamprophyres and mineralogy of lamproites are reported from the Denizli region, Western Anatolia, Turkey (Semiz et al., 2012), Karinya Syncline, Western Australia (Muller et al., 1993), Mt. Bundey area, NW Territories, Australia (Sheppard and Taylor, 1992) and from the Polayapalle area, Eastern Dharwar Craton, southern India (Madhavan et al., 1998; Chalapathi Rao et.al., 2008). Therefore, we prefer to place the Jharia and Raniganj ultrapotassic rocks under the same category and their petrogenetic and geodynamic aspects would be assessed in the ensuing sections.

6.1. Crustal contamination and assimilation

Petrographic as well as megascopic studies do not reveal entrained crustal xenoliths in the studied samples. Major-oxide compositions reveal low silica (SiO_2: 29.27–45.93), alumina (Al_2O_3: 4.03–8.25 wt.%) and extremely low sodium ($Na_2O \ll 0.76$ wt.% with the exception of JH8/BH2 sample which has high modal clinopyroxene and amphibole thereby elevating Na_2O to 1.2 wt.%; Table 9). As the ultrapotassic

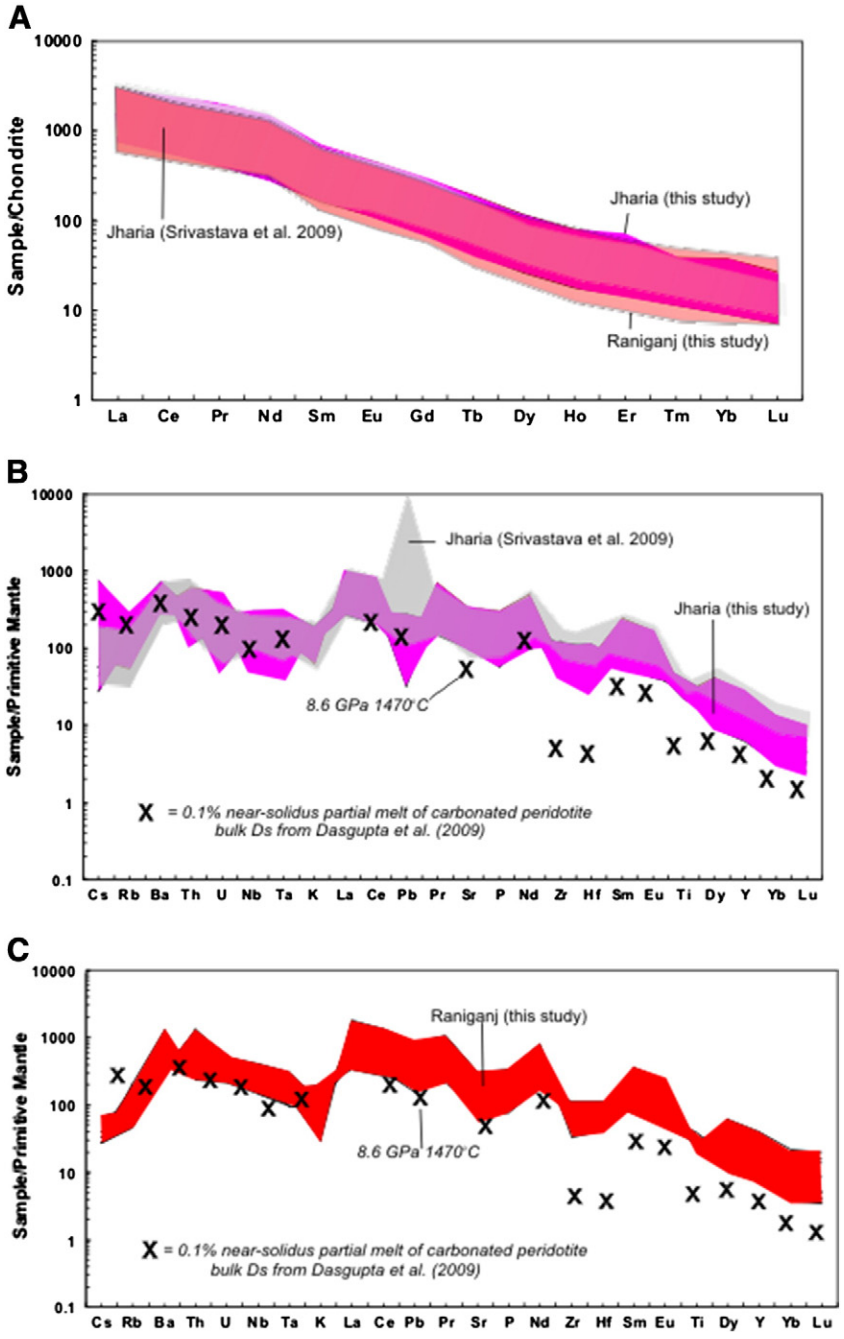

Fig. 6. (A) Chondrite-normalised (after Evensen et al., 1978) rare earth element distribution pattern fields for the samples under study. The data for Jharia samples reported by Srivastava et al. (2009) is also shown. Primitive mantle normalised (Palme and O'Neill, 2003) multi-element patterns for (B) Jharia samples of this study compared with those reported by Srivastava et al. (2009) and (C) Raniganj samples. The crosses in (B) and (C) represent calculated trace element patterns for near-solidus partial melts of carbonated peridotite at 8.6 GPa (Dasgupta et al., 2009). The model patterns were obtained by using the experimentally determined bulk peridotite/melt partition coefficients and a 0.1% batch partial melting model and taken from Tappe et al. (2013).

Table 11
Sr and Nd isotopic data of the samples under study.

S. no.	Sample	Rb (μg/g)	Sr (μg/g)	$^{87}Rb/^{86}Sr$	$^{87}Sr/^{86}Sr_m$	$^{87}Sr/^{86}Sr_i$[a]	Sm (μg/g)	Nd (μg/g)	$^{147}Sm/^{144}Nd$	$^{143}Nd/^{144}Nd_m$[a]	$^{143}Nd/^{144}Nd_i$	εNd	T_{DM} (Ma)
1	JH6/12[b]	144	393	1.06	0.70635 ± 28	0.704637 ± 28	38.8	261	0.0899	0.512404 ± 36	0.512337 ± 36	−3.0	900
2	JH8/BH2[b]	172	441	1.12	0.70679 ± 28	0.704966 ± 28	15.9	101	0.0953	0.512387 ± 36	0.512316 ± 36	−3.4	963
3	RGM09/8[b]	125	106	3.41	0.71844 ± 28	0.712919 ± 28	45.3	209	0.0943	0.512366 ± 36	0.512268 ± 36	−4.4	1426
4	JH8/7B[b]	183	301	1.76	0.70809 ± 28	0.705247 ± 28	16.7	108	0.0935	0.512442 ± 36	0.512372 ± 36	−2.3	883
Standard	BCR2	43	324	0.384	0.70506 ± 28		6.69	27.4	0.1477	0.512622 ± 36			
Standard	W2	23.3	193	0.348	0.70700 ± 28		3.51	13.8	0.154	0.512507 ± 36			

[a] 2σ errors on least significant digits.
[b] Samples leached in 2 N HCl.

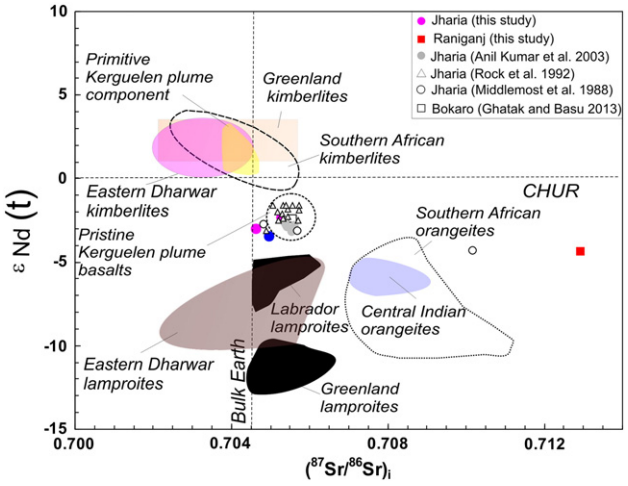

Fig. 7. $\varepsilon_{Nd}(t)$ values versus $^{87}Sr/^{86}Sr_i$ ratios (adapted from Tappe et al., 2011) for Jharia and Raniganj samples investigated in this study compared with the available data for such rocks from the Damodar valley. Data sources: Primitive Kerguelen plume component field is from Ghatak and Basu (2013); Pristine Kerguelen plume basalts field is from Weis et al. (1998); Eastern Dharwar craton kimberlites from Chalapathi Rao et al. (2013); Krishna lamproites (Chalapathi Rao et al., 2004; Chakrabarti et al., 2007); Mesozoic southern African kimberlites and orangeites (Nowell et al., 2004); Mesoproterozoic Labrador lamproites (Tappe et al., 2007); Mesoproterozoic Greenland lamproites (Nelson, 1992); Behradih and Kodomali orangeites, Central India (Lehmann et al., 2010; Chalapathi Rao et al., 2011) and Neoproterozoic Greenland kimberlites (Tappe et al., 2011).

rocks intrude sandstones and shales of the Gondwana sedimentary basins via continental crust, assimilation of felsic minerals such as quartz and feldspar derived from either of these provenances should have resulted in a marked elevation of silica, alumina and sodium. Rather, the abundance of incompatible elements such as Sr (up to 8805 ppm), Zr (up to 1320 ppm) and Nb (up to 244 ppm) are several orders higher compared to abundances in the continental crust. High La/Yb ratios (85–145) and absence of positive Eu spikes, further argue against significant assimilation of crustal material. Strikingly similar normalised REE as well as multi-element patterns (Fig. 6A and B) amongst samples from Jharia and Raniganj also exclude crustal contamination since systematic similarities or differences cannot be accounted by the latter.

Even though Ce and Nb contents of the samples of this study are much higher (Fig. 8A and B) than those of average sub-continental lithospheric mantle (SCLM), and supposedly uncontaminated mantle reservoirs such as MORB and OIB, their Ce/Pb and Nb/U ratios (which are relatively unaffected by fractionation) display far a greater spread and the latter display weak subduction-related trends (Fig. 8B). It should be pointed out here that the Jharia samples earlier studied by us (Srivastava et al., 2009) have elevated Pb contents (marked by a pronounced positive Pb spike in Fig. 6B) thereby resulting in their lower Ce/Pb ratios similar to those of pelagic sediments (Fig. 8A). As crustal contamination has been inferred to be minimal (above), we attribute the lower Nb/U and Ce/Pb in the studied samples to be primary. As the Nb/Yb values of the Damodar Valley samples are too high and Th/Yb values too low compared to that of a mantle source containing a subducted crustal component (Fig. 8C), they are confined to the mantle array defined by the average composition of N-MORB, E-MORB and OIB. Thus, both plume- and subduction-derived components are inferred as sources to the Damodar Valley ultrapotassic rocks, but with a greater contribution from plume-related components.

6.2. Mantle source region, enrichment and genesis

Mantle xenoliths or their disaggregated xenocrysts were not observed in rocks of the study area. In fact, there is only one report of mantle xenolith of harzburgitic nature containing olivine, orthopyroxene and chrome spinel recorded from the ultrapotassic rocks of Damodar Valley (Basu et al., 1997). The reported xenoliths are up to 2 cm in diameter and are pear and discoid in shape. No further information is available on them. Lack of olivine and its compositional data does not permit us to evaluate the composition of primary magma that equilibrated with the mantle source of the ultrapotassic rocks from the Damodar Valley. It is well established that primary magmas have Mg# = 65–85 Ni = 90–700 ppm, Co = 25–80 ppm, Sc = 15–30 ppm, Cr = 200–500 ppm and $SiO_2 < 50$ wt.% (e.g. Frey et al., 1978; Foley et al., 1987; Rock, 1991). Majority of data of this study (Tables 9 and 10) are confined to this

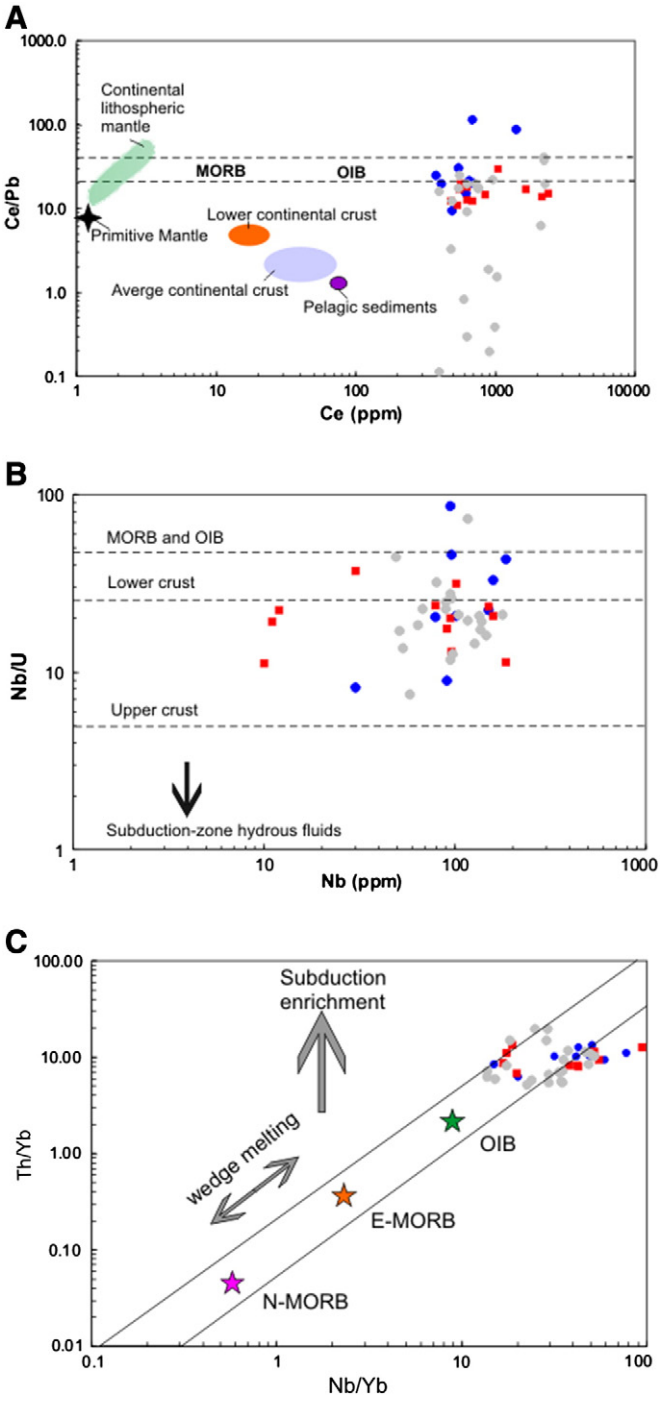

Fig. 8. (A), Ce (ppm) vs Ce/Pb diagram for the samples under study and various fields are taken from Owen (2008); (B) Nb/U vs. Nb diagram for the samples under study and various fields are taken from Ma et al. (2013) and the references therein. (C) Nb/Yb versus Th/Yb plot for the samples under study showing the MORB-OIB mantle array as well as vectors for enrichment related to subduction and wedge melting (from Pearce, 2008). The symbols in all the three plots remain the same as in Fig. 4A.

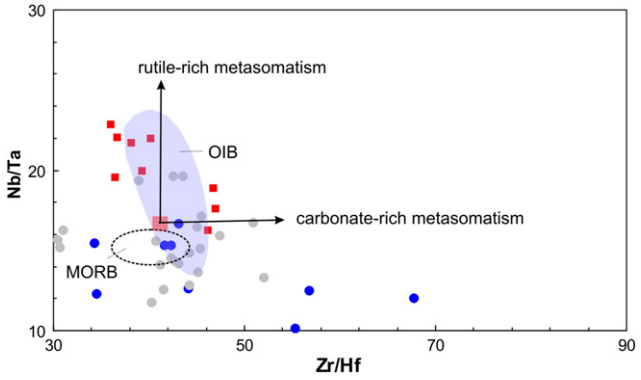

Fig. 9. Zr/Hf vs Nb/Ta plot for the samples under study showing possible rutile and carbonate-enrichment processes in the source. Symbols remain the same as in Fig. 4A and various other fields and data sources are from Guo et al. (2004).

range implying the primary character of their magmas. However, a few of the samples have lower Mg#, Ni and Cr values highlighting the role of olivine + phlogopite + spinel ±clinopyroxene ± amphibole fractionation. The variability of the fractionating phases can account for the petrological and geochemical differences amongst the studied samples.

Geochemical parameters such as high Mg#, elevated concentration of compatible elements such as Ni, Cr and Co, and low concentration of HREE imply a refractory source, akin to a depleted harzburgite, which would have experienced previous melt extraction (e.g. McCall et al., 1990; Le Roex and Lanyon, 1998; Beard et al., 2000; Mirnejad and Bell, 2006) in the generation of the Damodar Valley ultrapotassic magma. Widespread occurrence of Precambrian mafic dykes (Kumar and Ahmad, 2007; Srivastava et al., 2012 and references therein) and recently reported komatiites from the Chhotanagpur Gneissic Terrane (Bhattacharya et al., 2010) provide evidence for such previous melt extraction. In contrast, high abundances of incompatible trace elements i.e. LILE and HFSE in the samples clearly suggest their subsequent enrichment and thus require an 'enriched' mantle source—which is further corroborated by their negative ε_{Nd} values. Therefore a previously depleted as well as subsequently enriched mantle source, similar to that commonly envisaged as the source regions of kimberlites and lamproites (e.g. Tainton and McKenzie, 1994; Becker and Le Roex, 2006) is valid for the Damodar Valley ultrapotassic rocks. Higher concentrations of LREE relative to HREE as well as relatively high concentrations of

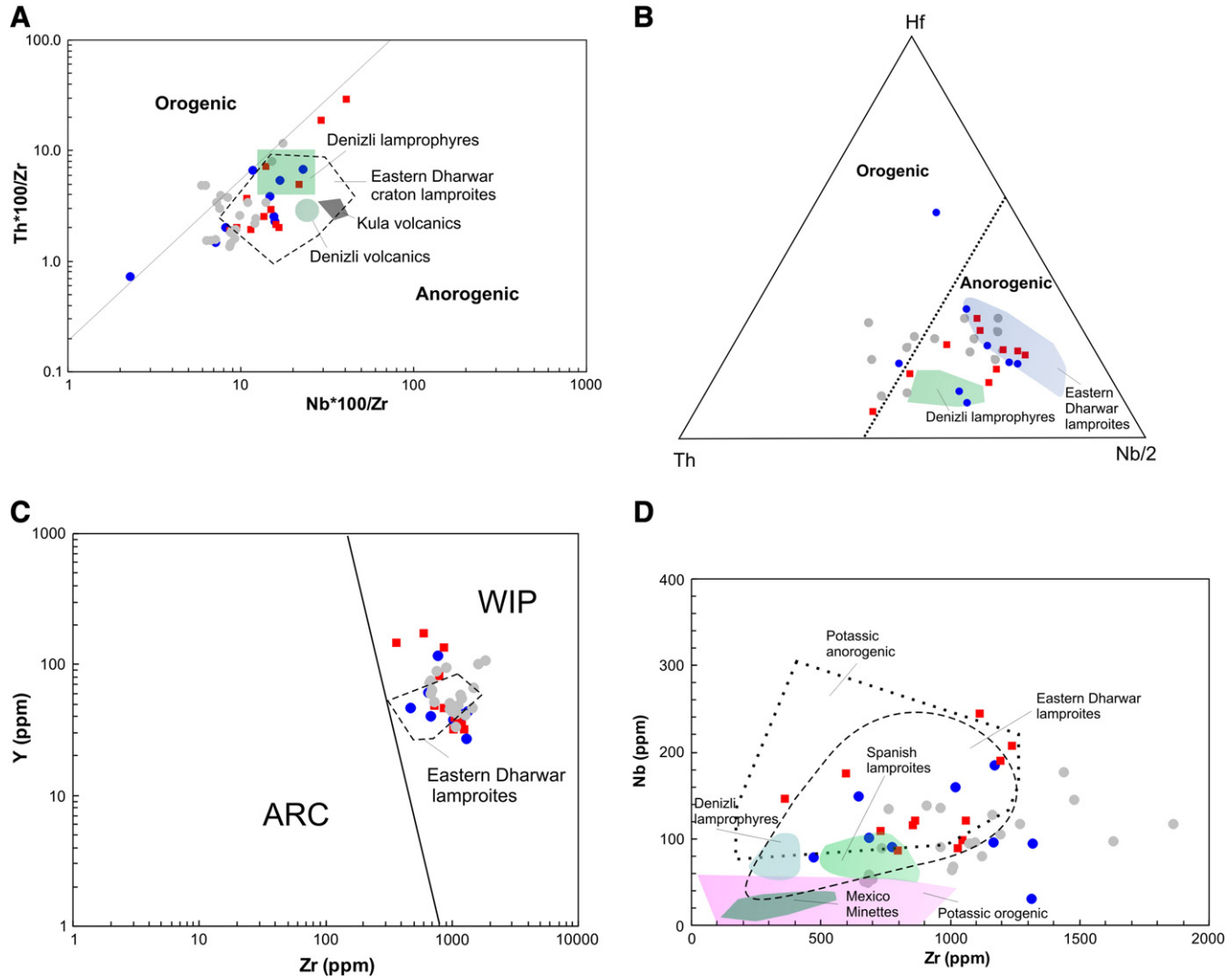

Fig. 10. Discrimination diagrams deploying (A) Nb/Zr vs Th/Zr (B) Hf–Th–Nb,(C) Zr (ppm) vs Y (ppm) and (D) Zr (ppm) vs Nb (ppm) to distinguish between anorogenic and orogenic settings for potassic rocks (various fields are sourced from Muller and Groves, 2000; Semiz et al., 2012 and references therein). The field of Eastern Dharwar craton lamproites is from Chalapathi Rao et al. (2004, 2010) and Paul et al. (2007).

compatible elements also imply generation of magma from such a metasomatised (enriched) mantle source by small degrees of partial melting within the garnet stability fields (e.g. Hirschmann et al., 1999; Dasgupta et al., 2009).

There is little consensus on the provenance of the melts and fluids responsible for mantle metasomatism and a variety of models are in vogue: (i) subducted oceanic lithosphere (e.g. Coe et al., 2008; Garza et al., 2013), (ii) convective (asthenospheric) mantle (e.g. McKenzie, 1989; O'Brien et al., 1991) (iii) deep-mantle plumes (Collerson et al., 2010; Torsvik et al., 2010) and (iii) cratonic lithosphere (e.g., Beccaluva et al., 2001; Tappe et al., 2007; Foley, 2008). Likewise, the composition of the melts and fluids leading up to mantle metasomatism is also widely debated, based on mineralogical, chemical and isotopic composition of mantle xenoliths, and ranges from carbonate and alkali-rich silicate melts to H_2O- and CO_2-rich fluids (e.g., Frey and Green, 1974; Coltorti et al., 1999; Ionov et al., 2002). The depleted-mantle (T_{DM}) Nd model ages (which are minimum ages) indicate that the source enrichment of these rocks occurred at 970–1450 Ma (Table 11). An l ~ 1 Ga interval between source enrichment and dyke emplacement traces such an enriched source to be within the sub-continental lithospheric mantle (SCLM), rather than in a convecting mantle source. These model ages are indistinguishable to the emplacement ages (1.1–1.4 Ga) of the Eastern Dharwar Craton kimberlites and lamproites (Chalapathi Rao et al., 2013b, 2013c) as well as with the timing (~1.1 Ga) of source-enrichment of the recently discovered orangeites from the Bastar craton, Central India (Chalapathi Rao et al., 2011) thereby implying a geologically significant regional metasomatic event. Therefore, we do not favour interpreting the older Nd model ages to result from re-cycled material tapped upon melting in the asthenosphere vis-à-vis Kerguelen mantle plume, but attribute the older model ages to the ~1.1 Ga regional metasomatic event. The Raniganj samples are characterised by a higher Nb/Ta and lesser Zr/Hf compared to those from the Jharia and display affinities towards rutile- as well as carbonate-rich metasomatism (Fig. 9) whereas Jharia samples show strong affinities towards carbonate-rich metasomatism. Introduction of a CO_2-rich fluid in a depleted mantle source can elevate LREE relative to HREE (Barbieri et al., 1997) and also presence of Sr-rich apatite and carbonate-rich nature of the studied rocks possibly provide additional support for the metasomatism by CO_2-rich fluids or carbonatitic melts (see Hauser et al., 2010). Likewise, high modal rutile in the studied rocks points towards rutile-rich metasomatism. Thus, the involvement of carbonate- as well as rutile-rich metasomatism, presumably related to Kerguelen mantle plume, in the genesis of the Damodar Valley ultrapotassic rocks is inferred from petrological as well as geochemical grounds.

Recently Tappe et al. (2013) used a new set of 'bulk' peridotite/melt partition coefficients, reported by Dasgupta et al. (2009), to calculate trace element patterns for partial melting of a carbonated peridotite source between 6 and 10 GPa utilizing a fixed 0.1% batch partial melting model (McKenzie, 1985; Gudfinnsson and Presnall, 2005) and source trace element contents set at primitive mantle values (Palme and O'Neill, 2003). Tappe et al. (2013) have shown that the calculated trace element compositions remarkably match with those from the analyzed Eocene-aged Lac de Gras kimberlites of Canada and infer their derivation from low-degree partial melting of carbonated peridotite under convective mantle conditions. By deploying the melting model of Tappe et al. (2013) to the Jharia and Raniganj samples, a very good fit for many of the incompatible trace elements is observed, with the exception of Zr–Hf, Ti and HREE (all of which show a poorer fit owing to their derivation from shallower depths and lesser control of garnet as a HREE controlling phase), (Fig. 6B and C) indeed suggesting the involvement of a carbonated peridotite in their petrogenesis. Our findings are consistent with (i) quenching experiments on a few of the Jharia ultrapotassic rocks which envisage their crystallisation from a highly potassic, silica-undersaturated magma dominated by fluids rich in H_2O and CO_2 (Gupta et al., 1983) and (ii) involvement of relatively primitive carbonated garnet peridotite source in the Kerguelen plume (Ghatak and Basu, 2013).

6.3. Tectonic implications

The eruption ages of the potassic–ultrapotassic rocks serve as time-capsules and are of tectonomagmatic significance (e.g., Heaman et al., 2004; Chalapathi Rao, 2007; Jelsma et al., 2009). As there is no direct field relationship between the Rajmahal Traps and ultrapotassic rocks of the Damodar Valley it is not possible to ascertain their relative stratigraphic ages. The most precise radiometric ages are available for only a few ultrapotassic samples from the Jharia and they range from 114 to 116 Ma (Kent et al., 1998; P.R. Renne in Ghatak and Basu, 2013) and appear to slightly post-date the eruptive ages of 117–118 Ma available for the Rajmahal and Sylhet Traps (Baksi, 1995; Ray et al., 2005). Given the availability of very limited isotopic ages and uncertainties in precision, we consider that this age correlation can only be a first order inference.

Recent geochemical and radiogenic (Nd–Sr–Pb) isotopic studies on a variety of mafic–ultramafic–alkalic–carbonatitic complexes in a widespread area of one million km^2 in the eastern and NE India demonstrate their compelling linkage with the Kerguelen mantle plume (Ghatak and Basu, 2013). Initially the Kerguelen mantle plume was considered to have acted as a heat source for the Rajmahal and Sylhet Traps (Mahoney et al., 1983; Kent et al., 1997) but subsequently its role also as their magma feeder has been recognised (Storey et al., 1992; Ingle et al., 2002; Ghatak and Basu, 2013). However, the relative contribution of Kerguelen plume and sub-continental lithospheric components in the generation of Damodar Valley ultrapotassic rocks remains unclear with existing models envisaging them either a) as solely lithospheric-derived melts (Middlemost et al., 1988; Kent et al., 1998; Mitchell and Fareeduddin, 2009), b) of asthenospheric (Kerguelen-plume related) derivation (Kumar et al., 2003) or c) even their combination in varying proportions (Srivastava et al., 2009; Ghatak and Basu, 2013). A number of discrimination plots using the High-Field Strength Elements (Fig. 10A–D) suggest predominantly within-plate (anorogenic) and plume-type tectonic setting (see also Fig. 8A–C) for these ultrapotassic rocks, also consistent with their cratonic nature. However, some Jharia samples also display subduction-related characteristics (Fig. 10A and B) as also highlighted in an earlier section (above; see Figs. 6B, C and 8A, B); we infer these geochemical patterns to be related to long-term memories of ancient (Archaean) subduction being events at the northern margin of the Singhbhum craton (see Jia et al., 2003; Srivastava et al., 2009). These geochemical characteristics, coupled with differences in the multi-element trace element patterns (Fig. 6B and C), are strong evidence for involvement of heterogeneous mantle in the petrogenesis of the Damodar Valley ultrapotassic dykes which is also supported by a pronounced time gap of ~500 Ma in their source enrichment (Table 10).

7. Conclusions

The studied ultrapotassic rocks from the Jharia and Raniganj basins in Damodar Valley, eastern India, display considerable textural diversity and yet portray coherent within-basin geochemical similarity highlighting their co-genetic nature. Their bulk-geochemical and petrographic characteristics resemble those of ultramafic lamprophyres (aillikites) whereas mineral composition is closer to that of lamproites and rarely that of orangeites and kimberlites. The existing alkaline rock nomenclature schemes are grossly inadequate to characterise them. The studied rocks are strikingly comparable to similar such rocks having affinities to lamprophyres and lamproites and reported from elsewhere at Denizli region (Western Anatolia, Turkey), Karinya Syncline and Mt. Bundey (Australia) and the Polayapalle, eastern Dharwar craton (southern India). The ultrabasic nature coupled with low sodium and alumina contents together with high incompatible trace element abundances and

their ratios reveal a limited influence of crustal contamination. Involvement of a predominantly plume and minor subduction-related component has been inferred from geochemical discrimination plots. Sr–Nd_i isotopic ratios of the Damodar Valley ultrapotassic rocks imply their derivation from source regions with long term incompatible element enrichment relative to that of Bulk Earth and contrast with those of kimberlites and orangeites from India and southern Africa as well as primitive Kerguelen plume component but indistinguishable from those of the pristine Kerguelen mantle plume derived basalts. Their depleted mantle (T_{DM}) model ages (0.95–1.4 Ga) are overlap with those of the Deccan-age orangeites from the Bastar craton, central India, and the emplacement ages (1.1–1.4 Ga) of kimberlites and lamproites from the eastern Dharwar craton, southern India thereby implying a regional metasomatic event. The ultrapotassic rocks of this study represent small degree-partial melts derived from a depleted garnet bearing harzburgitic source which has experienced metasomatism by carbonate- and rutile-rich fluids/melts via Kerguelen plume. A temporal difference of ~500 Ma in the source enrichment of Jharia and Raniganj ultrapotassic rocks coupled with distinct incompatible element signatures bring out involvement of heterogeneous mantle source (s) in their genesis.

Acknowledgements

The Head, Department of Geology, BHU, is thanked for his support and encouragement. The Department of Science and Technology, New Delhi is thankfully acknowledged for providing research grant for the present work (ESS/16/299/2006). Thanks are also due to various coal mine owners in the Damodar valley for permitting us to sample from their mines and at times for generously providing us with drill core samples at their disposal. Insightful reviews by Ray Kent (Leicester), Sebastian Tappe (Johannesburg) and an unknown referee as well as editorial suggestions by Mike Widdowson (London) are deeply appreciated.

References

Acharyya, S.K., 2003. The nature of Mesoproterozoic central Indian tectonic zone with exhumed and reworked older granulites. Gondwana Res. 6, 197–214.
Agarwal, J., Rama, K., 1976. Chronology of Mesozoic volcanics in India. Proc. Indian Acad. Sci. 84A, 157–179.
Baksi, A.K., 1995. Petrogenesis and timing of volcanism in the Rajmahal flood basalt province, northeastern India. Chem. Geol. 121, 73–90.
Baksi, A.K., Barman, T.R., Paul, D.K., Farrar, E., 1987. Widespread early Cretaceous flood basalt volcanism in Eastern India: geochemical data from the Rajmahal–Bengal–Sylhet Traps. Chem. Geol. 63, 133–141.
Basu, A., Bhattacharya, A.K., Paul, D.K., 1997. Petrology and geochemistry of the lamprophyric rocks from the Bokaro Coal field, Bihar and their economic potential. J. Geol. Soc. India 50, 255–266.
Barbieri, M., Ghiara, M.R., Stanzione, D., Viklar, L.M., Pezzuti, N.E., Segal, S.J., 1997. Trace-element and isotope constraints on the origin of ultramafic lamprophyres from Los Alisos (Sierra Subandinas, Northern Argentina). Journal of South American Earth Sciences 10, 39–47.
Beard, A.D., Downes, H., Hegner, E., Sablukov, S.M., 2000. Geochemistry and mineralogy of kimberlites from the Arkhangelsk region, NW Russia: evidence for transitional kimberlite magma types. Lithos 51, 47–73.
Beccaluva, L., Bonadiman, C., Coltorti, M., Salvini, L., Siena, F., 2001. Depletion events, nature of metasomatizing agent and timing of enrichment processes in lithospheric mantle xenoliths from the Veneto Volcanic Province. J. Petrol. 42, 173–187.
Becker, M., Le Roex, A.P., 2006. Geochemistry of South African on- and off-craton Group I and II kimberlites: petrogenesis and source region evaluation. J. Petrol. 47, 673–703.
Bhattacharya, D.K., Mukherjee, D., Barla, V.C., 2010. Komatiite within Chhotanagpur Gneissic Complex at Semra, Palmau district, Jharkhand: petrological and geochemical fingerprints. J. Geol. Soc. India 76, 589–606.
Blandford, W.T., 1861. On the geological structure and relations of the Raniganj coal field. Indian Miner. 1, 9–29.
Bose, P.N., 1888. Notes on some mica traps from Barakar and Raniganj. Rec. Geol. Surv. India 21, 163.
Bratzdrum, C., Grapes, R., Giere, R., 2009. Late-stage hydrothermal alteration and heteromorphism of calc-alkaline lamprophyre dykes in Late Jurassic Granite, Southeast China. Lithos 113, 820–830.
Brod, J.A., Gasper, J.C., Aruajo, D.P.D., Gibson, S.A., Thompson, R.N., Brod, T.C.J., 2001. Phlogopite and tetra-ferriphlogopite from Brazilian carbonatite complexes: petrogenetic constraints and implications for mineral-chemistry systematics. J. Asian Earth Sci. 19, 265–296.
Chakrabarti, R., Basu, A.R., Paul, D.K., 2007. Nd–Hf–Sr–Pb isotopes and trace element geochemistry of Proterozoic lamproitesfrom southern India: subducted komatiite in the source. Chem. Geol. 236, 291–302.
Chakraborty, C., Mandal, N., Ghosh, S.K., 2003. Kinematics of the Gondwana basins of peninsular India. Tectonophysics 377, 299–324.
Chalapathi Rao, N.V., 2007. Chelima dykes, Cuddapah Basin, Southern India: a review of the age, petrology, geochemistry and petrogenesis of the worlds' oldest lamproites. J. Geol. Soc. India 69, 523–538.
Chalapathi Rao, N.V., 2008. Precambrian alkaline potassic–ultrapotassic, mafic–ultramafic magmatism in Peninsular India. J. Geol. Soc. India 72, 57–82.
Chalapathi Rao, N.V., 2011. Sr-rich apatite and Nb-rutile from the Chelima lamproite dykes, Cuddapah basin, southern India and their petrological significance. Curr. Sci. 100, 1207–1210.
Chalapathi Rao, N.V., Lehmann, B.L., 2011. Kimberlites, flood basalts and mantle plumes: new insights from the Deccan large Igneous Province. Earth Sci. Rev. 107, 315–324.
Chalapathi Rao, N.V., Gibson, S.A., Pyle, D.M., Dickin, A.P., 2004. Petrogenesis of Proterozoic kimberlites and lamproites from the Cuddapah basin and the Dharwar craton, southern India. J. Petrol. 45, 907–948.
Chalapathi Rao, N.V., Kamde, G., Kale, H.G., Dongre, A., 2010. Mesoproterozoic lamproites from the Krishna Valley, Eastern Dharwar craton, southern India: petrogenesis and diamond prospectivity. Precambrian Res. 177, 103–130.
Chalapathi Rao, N.V., Lehmann, B., Mainkar, D., Belyatsky, B., 2011. Petrogenesis of the end-Cretaceous diamondiferous Behradih kimberlite pipe, Bastar craton: implication for mantle–plume lithosphere interaction in Central India. Contrib. Mineral. Petrol. 161, 721–742.
Chalapathi Rao, N.V., Kumar, S., Sinha, A., Srivastava, R.K., 2013a. K-rich titanate from the Jharia ultrapotassic rock, Damodar valley, Eastern India and its petrological significance. J. Geol. Soc. India 81, 733–736.
Chalapathi Rao, N.V., Wu, F.Y., Mitchell, R.H., Li, L.Q., Lehmann, B., 2013b. Mesoproterozoic U–Pb ages, trace element and Sr–Nd isotopic composition of perovskite from kimberlites of the Eastern Dharwar craton, southern India: distinct mantle sources and a widespread 1.1 Ga tectonomagmatic event. Chem. Geol. 353, 48–64.
Chalapathi Rao, N.V., Creaser, R.A., Lehmann, B., 2013c. Re–Os isotope study of Indian kimberlites and lamproites: implications for their mantle source regions and cratonic evolution. Chem. Geol. 353, 36–47.
Coe, N., Le Roex, A.P., Gurney, J.J., Pearson, G., Nowell, G., 2008. Petrogenesis of the Swartruggens and Star Group II kimberlite dyke swarms, South Africa: constraints from whole rock geochemistry. Contrib. Mineral. Petrol. 156, 627–652.
Collerson, K.D., Williams, Q., Ewart, A.E., Murphy, D.T., 2010. Origin of HIMU and EM-1 domains sampled by ocean island basalts, kimberlites and carbonatites: the role of CO_2-fluxed lower mantle melting in thermochemical upwellings. Phys. Earth Planet. Inter. 181, 112–131.
Coltorti, M., Bonadiman, C., Hinton, R.W., Siena, F., Upton, B.G.J., 1999. Carbonatite metasomatism of the oceanic upper mantle: evidence from clinopyroxenes and glasses in ultramafic xenoliths of Grande Comore, Indian Ocean. J. Petrol. 40, 133–165.
Conticelli, S., 1988. The effect of crustal contamination on ultrapotassic magmas with lamproitic affinity: mineralogical, geochemical and isotope data from the Torre Alfina lavas and xenoliths, central Italy. Chem. Geol. 149, 51–81.
Dasgupta, R., Hirschmann, M.M., McDonough, W.F., Spiegelman, M., Withers, A.C., 2009. Trace element partitioning between garnet lherzolite and carbonatite at 6.6 and 8. 6 GPa with applications to the geochemistry of mantle and mantle-derived melts. Chem. Geol. 262, 57–77.
Edgar, A.D., 1989. Barium- and strontium-enriched apatites in lamproites from West Kimberley, Western Australia. Am. Mineral. 74, 889–895.
Ernst, R.E., Srivastava, Rajesh K., 2008. India's place in the Proterozoic world: constraints from the Large Igneous Province (LIP) record. In: Srivastava, R.K., Sivaji, Ch., Chalapathi Rao, N.V. (Eds.), Indian Dyes: Geochemistry, Geophysics and Geochronology. Narosa Publishers, pp. 413–445.
Evensen, N.M., Hamilton, P.J., O'Nions, R.K., 1978. Rare-earth abundances in chondritic meteorites. Geochim. Cosmochim. Acta 42, 1199–1212.
Foley, S.F., 2008. Rejuvenation and erosion of the cratonic lithosphere. Nat. Geosci. 1, 503–510.
Foley, S.F., Venturelli, G., Green, D.H., Toscani, L., 1987. The ultra-potassic rocks: characteristics, classification and constraints for petrogenetic models. Earth Sci. Rev. 24, 81–134.
Frey, F.A., Green, D.H., 1974. The mineralogy, geochemistry and origin of lherzolite Inclusions in Victorian basanites. Geochim. Cosmochim. Acta 38, 1023–1059.
Frey, F.A., Green, D.H., Roy, S.D., 1978. Integrated models of basalt petrogenesis: a study of quartz tholeiites to olivine melilites from southeastern Australia utilizing geochemical and experimental data. J. Petrol. 19, 463–513.
Frey, F.A., Weis, A.D., Borisova, A.Y., Xu, G., 2002. Involvement of continental crust in the formation of the Cretaceous Kerguelen Plateau: news perspectives from the ODP Leg 120 sites. J. Petrol. 43, 1207–1239.
Gale, G.H., Dabek, L.B., Fedikow, M.A.F., 1997. The application of rare earth element analyses in the exploration for volcanogenic massive sulphide type deposits. Explor. Min. Geol. 6, 233–252.
Garza, A.O., Dostal, J., Keppie, J.D., Moreno, F.A.P., 2013. Mid-Tertiary (25–21 Ma) lamprophyres in NW Mexico derived from subduction-modified subcontinental lithospheric mantle in an extensional backarc environment following steepening of the Benioff zone. Tectonophysics 590, 59–71.
Ghatak, A., Basu, A.R., 2011. The Sylhet Traps: vestiges of the Kerguelen plume in NE India. Earth Planet. Sci. Lett. 308, 52–64.

Ghatak, A., Basu, A.R., 2013. Isotopic and trace element geochemistry of alkalic–mafic–ultramafic–carbonatitic complexes and flood basalts in NE India: origin in a heterogeneous Kerguelen plume. Geochim. Cosmochim. Acta 115, 46–72.
Ghose, N.C., 1983. Geology, tectonics and evolution of the Chhotanagpur granite gneiss complex, Eastern India. In: Sinha-Roy, S. (Ed.), Structure and Tectonics of Precambrian rocks of India. Recent Researches in Geology, 10. Hindustan Publishing Corporation, Delhi, pp. 211–247.
Ghose, N.C., Mukherjee, D., Chatterjee, N., 2005. Plume generated Mesoproterozoic mafic–ultramafic magmatism in the Chotanagpur mobile belt of eastern Indian shield margin. J. Geol. Soc. India 66, 725–740.
Ghosh, S.C., 2006. The Raniganj coal basin: an example of an Indian Gondwana rift. Sediment. Geol. 147, 155–176.
Ghose, N.C., Chatterjee, N., 2008. Petrology, tectonic setting and source of dykes and related magmatic bodies in Chotanagpur gneissic complex, eastern India. In: Srivastava, R.K., Sivaji, Ch., Chalapathi Rao, N.V. (Eds.), Indian Dyke: Geochemistry, Geophysics and Geochronology. Narosa Publishing House Pvt Ltd., New Delhi, pp. 471–493.
Gibson, S.A., Thompson, R.N., Leonardos, O.H., Dickin, A.P., Mitchel, J.G., 1995. The Late Cretaceous impact of the Trindade mantle plume: evidence from large-volume, mafic, potassic magmatism in SE Brazil. J. Petrol. 36, 189–229.
Gibson, S.A., Thompson, R.N., Day, J.A., 2006. Timescales and mechanisms of plume–lithosphere interactions: $^{40}Ar/^{39}Ar$ geochronology and geochemistry of alkaline igneous rocks from the Parana-Etendeka large igneous province. Earth Planet. Sci. Lett. 251, 1–17.
Griffin, W.L., Natapov, L.M., O'Reilly, S.Y., van Achterbergh, E., Cherenkova, A.F., Cherenkov, V.G., 2005. The Kharamai kimberlite field, Siberia: modification of the lithospheric mantle by the Siberian Trap event. Lithos 81, 167–187.
Gudfinnsson, G.H., Presnall, D.C., 2005. Continuous gradations among primary carbonatitic, kimberlitic, melilititic, basaltic, picritic and komatiitic melts in equilibrium with garnet lherolite at 3–8 GPa. J. Petrol. 46, 1645–1659.
Guarino, V., Wu, F.Y., Lustrino, M., Melluso, L., Brotzu, P., Gomes, C.D.B., Ruberti, E., Tassinari, C.C.G., Svisero, D.P., 2013. U-Pb ages, Sr-Nd- isotope geochemistry, and petrogenesis of kimberlites, kamafugites and phlogopite-picrites of the Alto Paranaíba Igneous Province, Brazil. Chemical Geology 353, 65–82.
Guo, F., Fan, W., Wang, Y., Zhang, M., 2004. Origin of early Cretaceous calc-alkaline lamprophyres from the Sulu orogen in eastern China: implications for enrichment processes beneath continental collisional belt. Lithos 28, 291–305.
Gupta, A.K., Le Maitre, R.W., Haukka, M.L., Yagi, K., 1983. Geochemical studies on the carbonated apatite glimmerite, from Damodar valley, India. Proc. Jpn. Acad. Sci. B 59, 113–116.
Hastie, A.R., Kerr, A.C., Pearce, J.A., Mitchell, S.F., 2007. Classification of altered volcanic island arc rocks using immobile trace elements: development of the Th–Co discrimination diagram. J. Petrol. 48, 2341–2357.
Hauser, N., Matteini, M., Omarini, R.H., Pimentel, M.M., 2010. Constraints on metasomatised mantle under Central South America: evidence from Jurassic alkaline lamprophyre dykes from the Eastern Cordillera, NM Argentina. Mineral. Petrol. 100, 153–184.
Heaman, L.A., Kjarsgaard, B.A., Creaser, R.A., 2004. The temporal evolution of North American kimberlites. Lithos 76, 377–397.
Hirschmann, M.M., Ghiorso, M.S., Stolper, M., 1999. Calculation of peridotite partial melting from thermodynamic models of minerals and melts. II. Isobaric variations in melts near the solidus and owing to variable source composition. J. Petrol. 40, 297–313.
Ingle, S., Weis, D., Scoates, J.S., Frey, F.A., 2002. Relationship between the earlier Kerguelen plume and continental flood basalts of the paleo-eastern Gondwanan margins. Earth Planet. Sci. Lett. 197, 35–50.
Ionov, D.A., Bodinier, J.L., Mukasa, S.B., Zanetti, A., 2002. Mechanisms and sources of mantle metasomatism: major and trace element compositions of peridotite xenoliths from Spitsbergen in the context of numerical modelling. J. Petrol. 43, 2219–2259.
Jelsma, H.A., Barnett, W., Richards, S., Lister, G., 2009. Tectonic setting of kimberlites. Lithos 112s, 155–165.
Jia, Y., Kerrich, R., Gupta, A.K., Fyfe, W.S., 2003. 15 N-enriched Gondwana lamproites, eastern India: crustal N in mantle source. Earth Planet. Sci. Lett. 215, 43–56.
Kent, R.W., Ghose, N.C., Paul, P.R., Hassan, M.J., Saunders, A.D., 1992. Coal–magma interaction: an integrated model for the emplacement of cylindrical intrusions. Geol. Mag. 129, 753–762.
Kent, R.W., Saunders, A.D., Kempton, P.D., Ghose, N.C., 1997. Rajmahal basalt's, eastern India: mantle sources and melt distribution at a volcanic rifted margin. In: Mahoney, J. J., Coffin, M.F. (Eds.), Large Igneous Provinces: continental, oceanic and planetary flood volcanism. Geophys Monographs AGU, 100, pp. 145–182.
Kent, R., Kelley, S.P., Pringle, M.S., 1998. Mineralogy and $^{40}Ar/^{39}Ar$ geochronology of orangeites (Group II kimberlites) from the Damodar valley, eastern India. Mineral. Mag. 63, 313–323.
Kent, R.W., Pringle, M.S., Müller, R.D., Saunders, A.W., Ghose, N.C., 2002. $^{40}Ar/^{39}Ar$ geochronology of the Rajmahal basalts, India, and their relationship to the Kerguelen Plateau. J. Petrol. 43, 1141–1153.
Kumar, A., Ahmad, T., 2007. Geochemistry of mafic dykes in part of Chotanagpur gneissic complex: petrogenetic and tectonic implications. Geochem. J. 41, 173–186.
Kumar, Anil, Dayal, A.M., Padmakumari, V.M., 2003. Kimberlite from Rajmahal magmatic province: Sr–Nd–Pb isotopic evidence for Kerguelen plume derived magmas. Geophys. Res. Lett. 30, 2053. http://dx.doi.org/10.1029/2003GL018462.
Le Bas, M.J., 2000. IUGS reclassification of the high-Mg and picritic volcanic rocks. J. Petrol. 41, 1467–1470.
Le Maitre, R.W. (Ed.), 2002. Igneous Rocks: A Classification and Glossary of Terms. Recommendations of the International Union of Geological Sciences Subocmmission on the Systematics of Igneous Rocks. Cambridge University Press, Cambridge (236 pp.).
Le Roex, A.P., Lanyon, R., 1998. Isotope and trace element geochemistry of Cretaceous Damaraland lamprophyres and carbonatites, northwestern Namibia: evidence for plume–lithosphere interactions. J. Petrol. 39, 1117–1146.
Le Roex, A.P., Bell, D.R., Davis, P., 2003. Petrogenesis of Group I kimberlites from Kimberley, South Africa: evidence from bulk-rock geochemistry. J. Petrol. 44, 2261–2286.
Lehmann, B., Burgess, R., Frei, D., Belyatsky, B., Mainkar, D., Chalapathi Rao, N.V., Heaman, L.M., 2010. Diamondiferous kimberlites in Central India synchronous with the Deccan flood basalts. Earth Planet. Sci. Lett. 290, 142–149.
Luttinen, A.V., Zhang, X., Foland, K.A., 2002. 159 Ma Kjakebeinet lamproites (Dronning Maud Land, Antarctica) and their implications for Gondwana breakup Processes. Geol. Mag. 139, 525–539.
Ma, L., Jiang, S.Y., Hou, M.L., Dai, B.Z., Jiang, Y.H., Yang, T., Zhao, K.D., Pu, W., Zhu, Z.Y., Xu, B., 2013. Geochemistry of Early Cretaceous calc-alkaline lamprophyres in the Jiaodong Peninsula: Implication for lithospheric evolution of the eastern North China Craton. Gondwana Research 25, 859–872.
Madhavan, V., David, K., Rao, J.M., Chalapathi Rao, N.V., Srinivas, M., 1998. A comparative study of lamprophyres from the Cuddapah Intrusive Province (CIP). J. Geol. Soc. India 52, 621–642.
Mahadevan, T.M., 2002. Geology of Bihar and Jharkhand. Geological Society of India, Bangalore, (569 pp.).
Mahoney, J.J., MacDougall, J.D., Lugmair, G.W., Gopalan, K., 1983. Kerguelan hotspot source for Rajmahal Traps and Ninetyeast Ridge? Nature 303, 385–389.
Malpas, J., Foley, S.F., King, A.F., 1986. Alkaline mafic and ultramafic lamprophyres from the Aillik Bay area, Labrador. Can. J. Earth Sci. 23, 1902–1918.
Matchan, E., Hergt, J.M., Woodhead, J.D., Phillips, D., Shee, S.R., 2009. The geochemistry, petrogenesis ad age of an unusual alkaline intrusion in the western Pilbara craton, Western Australia. Lithos 112s, 419–428.
McCall, G.W., Nabelek, P.I., Bauer, R.L., Glascock, M.D., 1990. Petrogenesis of Archean lamprophyres in southern Vermilion Granitic Complex, northeastern Minnesota, with implications for the nature of their mantle source. Contrib. Mineral. Petrol. 104, 439–452.
McKenzie, D., 1985. Extraction of the magma from crust and the mantle. Earth Planet. Sci. Lett. 74, 81–91.
McKenzie, D., 1989. Some remarks on the movement of small melt fractions in the mantle. Earth Planet. Sci. Lett. 95, 53–72.
Melluso, L., Srivastava, R.K., Guarino, V., Zanetti, A., Sinha, A.K., 2010. Mineral chemistry and petrogenetic evolution of the ultramafic–alkaline–carbonatitic complex of Sung Valley, Northeastern India. Can. Mineral. 48, 205–229.
Melluso, L., Srivastava, R.K., Petrone, C.M., Guarino, V., Sinha, A.K., 2012. Mineralogy and magmatic affinity of the Jasra intrusive complex, Shillong Plateau, India. Mineral. Mag. 76, 1099–1117.
Middlemost, E.A.K., 1989. Iron oxidation ratios, norms and classification of volcanic rocks. Chem. Geol. 77, 19–26.
Middlemost, E.A.K., Paul, D.K., Fletcher, I.R., 1988. Geochemistry and mineralogy of the minette–lamproite association from the Indian Gondwana. Lithos 22, 31–42.
Mirnejad, H., Bell, K.K., 2006. Origin and Source Evolution of the Leucite Hills Lamproites: evidence from Sr–Nd–Pb–O Isotopic Compositions. J. Petrol. 47, 2463–2489.
Mitchell, R.H., 1995. Kimberlites, Orangeites and Related Rocks. Plenum Press, New York, (406 pp.).
Mitchell, R.H., 2006. Potassic magmas derived from metasomatised lithospheric mantle: nomenclature and relevance to exploration for diamond-bearing rocks. J. Geol. Soc. India 67, 317–327.
Mitchell, R.H., 2007. Potassic rocks from the Gondwana coal fields of India: closing Pandora's box of petrological confusion? J. Geol. Soc. India 69, 505–512.
Mitchell, R.H., Bergman, S.C., 1991. Petrology of Lamproites. Plenum Press, New York, (447 pp.).
Mitchell, R.H., Fareeduddin, 2009. Mineralogy of the peralkaline lamproites from the Raniganj coalfield, India. Mineral. Mag. 73, 457–477.
Morimoto, N., Fabries, J., Ferguson, A.K., Ginzburg, I.V., Ross, M., Siefert, F.A., Zussman, J., Aoki, K., Gottardi, G., 1988. Nomenclature of pyroxenes. Mineral. Mag. 52, 535–550.
Mukherjee, K.K., 1961. Petrology of the lamprophyres of Bokaro coalfield. Q. J. Mineral. Metall. Soc. India 33, 69–87.
Mukherjee, D., Ghose, N.C., 1999. Damodar graben: a centre of contrasting magmatism in the Eastern Indian shield margin. In: Sinha, A.K. (Ed.), Basement Tectoncis. Kluwer Academic Publishers, Dordrecht, pp. 179–202.
Mukhopadhyay, D., 1988. Precambrian of the eastern Indian shield. Geol. Soc. India Mem. 8, 237p.
Muller, D., Groves, D.J., 2000. Potassic Igneous Rocks and Associated Gold–copper Mineralization. Springer, Berlin, (252 pp.).
Muller, D., Morris, B.J., Farrand, M.J., 1993. Potassic alkaline lamprophyres with affinities to lamprophyres from the Karinya-Syncline, South Australia. Lithos 30, 123–138.
Naqvi, S.M., Rogers, J.J.W., 1987. Precambrian Geology of India. Oxford University Press, (223 pp.).
Nelson, D.R., 1992. Isotopic characteristics of potassic rocks—evidence for the involvement of subducted sediments in the magma. Lithos 28, 403–420.
Nowell, G.M., Pearson, D.G., Bell, D.R., Carlson, R.W., Smith, C.B., Kempton, P.D.M., Noble, S. R., 2004. Hf isotope systematics of kimberlites and their megacrysts: new constraints on their source regions. J. Petrol. 45, 1583–1612.
O'Brien, H.E., Irving, A.J., McCallum, I.S., 1991. Eocene potassic magmatism in the Highwood Mountains, Montana: petrology, geochemistry, and tectonic implications. J. Geophys. Res. 96, 13237–13260.
Owen, J.P., 2008. Geochemistry of lamprophyres from the Western Alps, Italy: implications for the origin of an enriched isotopic component in the Italian mantle. Contrib. Mineral. Petrol. 155, 341–362.

Palme, H., O'Neill, H.S.C., 2003. Cosmochemical estimates of mantle composition. In: Holland, H., Turekian, K.K. (Eds.), Treatise on Geochemistry, 2, pp. 1–38.
Paul, D.K., 2005. Petrology and geochemistry of the Salma dike, Ranigunj Coal field (Lower Gondwana), Eastern India: linkage with Rajmahal or Deccan volcanic activity? J. Asian Earth Sci. 25, 903–913.
Paul, D.K., Crocket, J.H., Reddy, T.A.K., Pant, N.C., 2007. Petrology and geochemistry including Platinum Group element abundances of the Mesoproterozoic ultramafic (lamproitic) rocks of Krishna district, southern India: implications for source rock characteristics and petrogenesis. J. Geol. Soc. India 69, 577–596.
Pearce, J.A., 2008. Geochemical fingerprinting of oceanic basalts with applications to ophiolite classification and the search for Archean oceanic crust. Lithos 100, 14–46.
Ravikant, V., 2010. Palaeoproterozoic (~1.9 Ga) extension and breakup along the eastern margin of the Eastern Dharwar craton, SE India: new Sm–Nd isochron age constraints from anorogenic mafic magmatism from the Neoarchaean Nellore greenstone belt. J. Asian Earth Sci. 37, 67–81.
Ray, J.S., Pattanayak, S.K., Pande, K., 2005. Rapid emplacement of the Kerguelen-plume related Sylhet Traps, eastern India: evidence from ^{40}Ar–^{39}Ar geochronology. Geophys. Res. Lett. 32, 1–4.
Reider, M., Cavazzini, D., Yakonov, Y.S.D., Frank-Kamenetskii, V.A., Gottardi, G., Guggenheim, S., Koval, P.V., Muller, G., Neiva, A.M.R., Radoslovich, E.W., Robert, J.L., Sassi, F.P., Takeda, H., Weiss, Z., Wones, D.R., 1998. Nomenclature of micas. Can. Mineral. 36, 905–912.
Rock, N.M.S., 1984. Nature and origin of calc-alkaline lamprophyres: minettes, vogesites, kersantites and spessartites. Trans. R. Soc. Edinb. 74, 193–227.
Rock, N.M.S., 1991. Lamprophyres. Blackie and Sons Ltd., Glasgow, (285 pp.).
Rock, N.M.S., Paul, D.K., 1989. "Lamprophyres", "lamproites" and "kimberlites" in India: a bibliography and preliminary reappraisal. Geol. Soc. India Mem. 15, 291–311.
Rock, N.M.S., Griffin, B.J., Edgar, A.D., Paul, D.K., Hergt, J.M., 1992. A spectrum of potentially dimondiferous lamproites and minettes from the Jharia coalfield, eastern India. J. Volcanol. Geotherm. Res. 50, 55–83.
Roeder, P.L., Schulze, D.J., 2008. Crystallization of groundmass spinel in kimberlite. J. Petrol. 49, 1473–1495.
Sarkar, A., Paul, D.K., Balasubrahmaniyan, M.N., Sengupta, N.R., 1980. Lamprophyres from Indian Gondwanas: K/Ar ages and chemistry. J. Geol. Soc. India 21, 188–193.
Schissel, D., Ernst, R.E., 2013. Kimberlites, carbonatites and LIPS: from SIPs to LIPs. http://convention.pdac.ca/pdac/conv/2013/pdf/ts/lip2-schissel.pdf.
Semiz, B., Coban, H., Roden, M.F., Ozpinar, Y., Flower, M.F.J., McGregor, H., 2012. Mineral composition in cognate inclusions in Late Miocene–Early Pliocene potassic lamprophyres with affinities to lamproites from Denizli region, Western Anatolia, Turkey: implications for uppermost mantle processes in a back-arc setting. Lithos 134–135, 253–272.
Shalivahan, Bhattacharya, B.B., Chalapathi Rao, N.V., Maurya, V.P., 2014. Thin lithosphere–asthnosphere boundary beneath eastern Indian craton. Tectonophysics 612–613, 128–133.
Sharma, R.S., 2009. Cratons and Fold Belts of India. Springer-Verlag, (304 pp.).
Sheppard, S., Taylor, W.R., 1992. Barium- and LREE-rich, olivine–mica–lamprophyres with affinities to lamproites, Mt. Bundey, Northern Territory, Australia. Lithos 28, 303–325.
Srivastava, R.K., Chalapathi Rao, N.V., 2007. Petrology, geochemistry and tectonic significance of Paleoproterozoic alkaline lamprophyres from the Jungel Valley, Mahakoshal supracrustal belt, Central India. Mineral. Petrol. 89, 189–215.
Srivastava, R.K., Sinha, A.K., 2007. Nd and Sr isotope systematics and geochemistry of plume related early Cretaceous alkaline–mafic–ultramafic igneous complex from Jasra, Shillong Plateau, Northeastern India. Geol. Soc. Am. Spec. Pap. 430, 815–830.
Srivastava, R.K., Heaman, L.M., Sinha, A.K., Shihua, S., 2005. Emplacement age and isotope geochemistry of Sung Valley alkaline–carbonatite complex, Shillong Plateau, northeastern India: implications for primary carbonate melt and genesis of the associated silicate rocks. Lithos 81, 33–54.
Srivastava, R.K., Chalapathi Rao, N.V., Sinha, A.K., 2009. Cretaceous potassic intrusives with affinities to aillikites from Jharia area: magmatic expression of metasomatically veined and thinned lithospheric mantle beneath Singhbhum craton, Eastern India. Lithos 112, 407–418.
Srivastava, R.K., Kumar, S., Sinha, A.K., 2012. Geochemical characteristics of Mesoproterozoic metabasite dykes from Chhotanagpur Gneissic Terrain, eastern India: implications for their emplacement in a plate margin tectonic emplacement. J. Earth Syst. Sci. 121, 509–523.
Srivastava, R.K., Kumar, S., Sinha, A.K., Chalapathi, Rao N.V., 2013. Petrology and geochemistry of high-titanium and low-titanium mafic dykes from the Damodar valley, Chhotanagpur Gneissic Terrain, eastern India and their relation to Cretaceous mantle plume(s). J. Asian Earth Sci. 84, 34–50.
Storey, M., Saunders, A.D., Tarney, J., Gibson, I., Norry, M.J., Thirlwall, M.F., Leat, P., Thompson, R.N., Menzies, M.A., 1989. Contamination of the Indian ocean asthenosphere by the Kerguelen-Head mantle plume. Nature 338, 574–576.
Storey, M., Kent, R.W., Saunders, A.D., Salters, V.J., Hergt, J., Whitechurc, H., Sevigny, J.H., Thirlwall, M.F., Leat, P., Ghose, N.C., Gifford, M., 1992. Lower Cretaceous rocks in continental margins and their relationship to the Kerguelen Plateau. Proc. Ocean Drill. Program Sci. Results 120, 33–53.
Tainton, K.M., McKenzie, D., 1994. The generation of kimberlites, lamproites and their source rocks. J. Petrol. 35, 787–817.
Tanaka, T., Togashi, S., Kamioka, H., Amakawa, H., Kagami, H., Hamamoto, T., Yuhara, M., Oribashi, Y., Yoneda, S., Shimuzu, H., Kuminaru, T., Takahashi, K., Yanagi, T., Nakano, T., Fujimaki, H., Shinjo, R., Asahara, Y., Tanimizu, M., Dragusanu, C., 2000. JNdi-1: a neodymium isotopic reference in consistency with La Jolla neodymium. Chem. Geol. 168, 279-28.
Tappe, S., Jenner, G.A., Foley, S.F., Heaman, L., Besserer, D., Kjarsgaard, B.A., Ryan, B., 2004. Torngat ultramafic lamprophyres and their relation to the North Atlantic Alkaline Province. Lithos 76, 491–518.
Tappe, S., Foley, S.F., Jenner, G.A., Kjarsgaard, B.C., 2005. Integrating ultramafic lamprophyres into the IUGS classification of igneous rocks: rationale and implications. J. Petrol. 46, 1893–2000.
Tappe, S., Foley, S.F., Stracke, A., Romer, R.L., Kjarsgaard, B.A., Heaman, L.M., Joyce, N., 2007. Craton reactivation on the Labrador Sea margins: $^{40}Ar/^{39}Ar$ age and Sr–Nd–Hf–Pb isotope constraints from alkaline and carbonatite intrusives. Earth Planet. Sci. Lett. 305, 235–248.
Tappe, S., Pearson, D.G., Nowell, G.M., Nielsen, T.F.D., Milstead, P., Muehlenbachs, K., 2011. A fresh isotopic look at Greenland kimberlites: cratonic mantle lithosphere imprint on deep source signal. Earth Planet. Sci. Lett. 305, 235–248.
Tappe, S., Pearson, D.G., Kjarsgaard, B.A., Nowell, G., 2013. Mantle transition zone input to kimberlite magmatism near a subduction zone: origin of anomalous Nd–Hf isotope systematics at Lac de Gras, Canada. Earth Planet. Sci. Lett. 371–372, 235–251.
Taylor, W.R., Kingdom, L., 1999. Mineralogy of the Jagersfontein kimberlite—an unusual Group I micaceous kimberlite- and a comment on the robustness of the mineralogical definition of 'orangeite'. Proceedings of the 7th International kimberlite conference, Cape Town (Nixon PH volume), pp. 861–866.
Torsvik, T.H., Burke, K., Steinberger, B., Webb, S.J., Ashwal, L.D., 2010. Diamonds sampled by plumes from the core–mantle boundary. Nature 466, 352–355.
Veena, K., Pandey, B.K., Krishna Murthy, P., Gupta, J.N., 1998. Sr and Nd isotopic systematics of the carbonatities of Sung Valley, Meghalaya, Northeast India: implications for contemporary plume-related mantle source characteristics. J. Petrol. 39, 1875–1884.
Verma, S.P., Torress-Alvarado, I.S., Sitelo-Rodriguez, Z.T., 2002. SINCLAS: Standard Igneous Norm and Volcanic Rock Classification System. Comput. Geosci. 28, 711–715.
Wagner, C., Velde, D., 1986. Mineralogy of K-richterite bearing lamproites. Am. Mineral. 71, 17–37.
Weis, D., Frey, F.A., Giret, A., Cantagrel, J.M., 1998. Geochemical characteristics of youngest volcano (Mont Ross) in the Kerguelen archipelago: inferences for magma mixing and composition of the Kerguelen plume. J. Petrol. 39, 973–994.
Woolley, A.L., Bergman, S.C., Edgar, A.D., Le Bas, M.J., Mitchell, R.H., Rock, N.M.S., Scott-Smith, B.H., 1996. Classification of lamprophyres, lamproites, kimberlites, and the kalsilitic, melilitic, and leucitic rocks. Can. Mineral. 34, 175–186.